Faculty of Science and Technology

MASTER'S THESIS

Study program/Specialization: Petroleum technology	Spring semester, 2022 Open
Writer: Sander Sunde Herlofsen	Sander Sunde Herlofsen (Writer's signature)
Faculty supervisor(s): Pål Østebø Andersen Reidar Inge Korsnes	
Title of master's thesis: Reactive flow with Sr-Ba-Mg brines in outcropped Mons chalk at reservoir conditions – experimental study	
Credits: 30	
Key words: Chalk, Core flooding experiments, Reaction kinetics, Steady state, IC analysis	Number of pages: 67 + Supplemental material: 0 Stavanger, 15.06.2022

Abstract

This experimental study investigated the reaction kinetics at various flow rates with Sr-, Ba-, Sr/Mg-, and Sr/Ba-based brines on outcropped Mons chalk. The experiment was carried out at a reservoir temperature equivalent to Ekofisk field (130°C), and a triaxial cell was used to withhold constant temperature, pore- and confining pressure.

Ion chromatographic analysis determined the ion compositions of effluent samples. The cores were flooded until effluent compositions no longer changed significantly over time before the injection rate was systematically changed between 0.5 and 8 PV/day. As the injection rate increased, the retention of divalent ions in the brine was expected to decrease and fewer calcium ions produced. The measured effluent concentrations were plotted and analyzed to understand how the flow rates affected the divalent ions retention in chalk and produced calcium from the chalk core.

The results showed that brine ions (strontium and barium) retained inside the core back-produced equal calcium concentration from the core and occurred in a substitution-like manner. Strontium ions were determined to have the highest retention with the chalk, with over 50 % of the original brine concentration precipitate inside the chalk core. Barium was determined to retain similar concentrations to previous experiments conducted on magnesium and barium. However, an unexpected increase in brine ion retention was measured for three of the brines (Ba, Sr/Mg, and Sr/Ba) when injecting flow rate above 1 PV/day, which could not be compared with results from previous studies.

Lastly, two of the cores were analyzed in a scanning electron microscope to observe the core's chemical composition at inlet and outlet after flooding over 100 days with reactive Sr- and Ba-based brines.

Acknowledgment

First and foremost, I would like to express my gratitude to Dr. Reidar Inge Korsnes for coaching me through the laboratory experiments. This thesis could not be conducted without his help to attend the experiments when I was working shift.

I would like to thank Dr. Pål Østebø Andersen and Korsnes guidance during the writing of this thesis. Their knowledge, expertise and motivation has been of great help and have always been available. It has been an honor to work with you.

I want to also express my sincere thanks to Dr. Mona Wetrhus Minde for conducting SEM analysis of the core findings.

Content

List of Figures

List of Tables

Nomenclature

CBE	Charge balance error
DW	Distilled water
IC	Ion chromatograph
LVDT	Linear variable differential transformer
LMA	Law of mass action
PV	Pore volumes
SEM	Scanning electron microscope
SSW	Synthetic seawater

1. Introduction

Carbonate lithology constitutes significant amounts of the hydrocarbon reserves. The Norwegian Continental Shelf fields, such as Ekofisk, Valhall, and Eldfisk, are carbonate reservoirs with chalk deposits. Chalk is a brittle, highly porous, and low permeable rock that consists mainly of calcite ($CaCO_3$). Chalk is reactive upon contact with reactive brine such as seawater or brines with similar compositions.

After years of production at Ekofisk field, the reservoir started to compact, and the seabed subsided due to the characteristics of chalk. Seabed subsidence on Ekofisk was first observed in 1984 and had subsided 10 feet since production started in 1971. Water injection was initiated in 1987 to repressurize and halt further subsidence. However, the subsidence continued after repressurizing the reservoir (Sulak & Danielsen, 1989; Sylte et al., 1999; Hermansen et al., 2000; Bjørlykke, 2015). After repressurizing the Ekofisk reservoir by water injection, the main contributor to subsidence was not the effective stresses but chalk-water interactions. Later studies proved that chalk compacts more when saturated in water than oil (Sylte et al., 1999). Hence, water changes the constitutive properties of chalk and mechanically weakens it (Doornhof et al., 2006).

Reservoir compaction and subsidence have affected drilling, casing deformation, pipelines, productivity, and production strategy, thereby causing high economic costs for the operators. Due to subsidence at the seabed, a decrease in platform airgap led to reduced platform safety. This was resolved in platform jacking operations and installing a barrier wall around the 2/4 T platform in 1987 and 1989. A combined cost of approximately $1 billion (Sulak, 1991; Nagel, 2001). Besides affecting surface structures, reservoir compaction has also affected wellbore safety. Casing deformation due to axial buckling or sub-horizontal shear in the overburden is an examples reservoir compaction which has ultimately required drilling a sidetrack. Moreover, pipelines exporting hydrocarbons from the platform to onshore may be laid through the tensile strain region on the flank of the subsidence or covered with rock dump. Therefore, exceeding the pipeline's design limits and requiring replacement or additional rock dumping (Nagel, 2001). Besides oilfield developing challenges regarding reservoir compaction and seabed subsidence,

a significant drive has come from compaction. The initial estimated oil recovery at Ekofisk was 17 %, but an updated oil recovery of the field is over 50 % due to compaction of the reservoir lithology and sea water injection (Oljedirektoratet, 2022). The significant increase in oil recovery for chalk fields with a high compaction drive, such as Ekofisk and Valhall, has resolved in extensive scientific studies regarding weakening and wettability effects on brine/seawater injection in chalk outcrops. In contrast, seabed subsidence and reservoir compaction continue to be a critical parameter in production strategy (Hermansen et al., 2000).

Seawater injection has proved to significantly affect oil recovery in chalk (Nagel, 2001; Minde, 2018; Mokhtari et al., 2022; Rendel et al., 2022). One factor studied on chalk inducing enhanced compaction drive is water weakening. Extensive core flooding studies have looked into the ion composition of the injection brine and how it affects chalk water weaking. Megawati et al. (2013) presented a rock mechanical test studying how intermolecular forces act upon chalk formation in the presence of sulfate at 50 and 130 °C. Their findings suggested that adsorption of sulfate ions causes a negative surface charge that gives rise to significant repulsive forces close to the inter granular contacts, accommodating local shear failures between grains and enhancing the pore collapse failures. In the presence of magnesium, it has been demonstrated the injected fluid leads to precipitation of new minerals, magnesium carbonate, and/or magnesium-bearing silicates. As a result, transport of calcium ions was observed in effluent samples and was interpreted as dissolution of calcite (Madland et al., 2011). The calcium/magnesium interaction has been investigated as a substitution-like behavior for the reason that the retained magnesium lost from the initial brine concentrations are of equal concentrations as calcium gain in effluent samples (Korsnes et al., 2006; Madland et al., 2011). Furthermore, Andersen & Berawala (2019) and Andersen et al. (2022) conducted a kinetic reaction modeling of this substitution-like behavior between calcium and magnesium from experimental data.

Nermoen et al. (2015) presented a long-term experiment studying dominating effects, rate of compaction, and dissolution, at different flow rates and how they affected porosity and permeability parameters. Sachdeva et al. (2019; 2020) studied the relation of wetting state and stiffness, strength, and time-dependent mechanical behavior with different deviant ions of Kansas and Mons chalk. In their study, it was observed that water-wet and wettability-altered

Mons samples had similar strength and stiffness. In contrast, the wettability-altered Kansas samples were stiffer and stronger than their water-wet counterparts. In both studies conducted by Sachdeva et al. (2019; 2020), various flow rates were performed to observe how it affected the objective of their study. Nermoen et al. (2015) and Sachdeva et al. (2019; 2020), even though reaction kinetics were not the main objective, observed that flow rates influenced compaction rate. Olsen's (2020) BSc- and Bukkholm's (2021) BSc thesis presented reactive flooding with magnesium conducted at different flow rates. Their studies observed lower concentrations of magnesium when the injection rate increased. Andersen et al. (2022) conducted an extensive study and modeling study of reaction kinetics of Olsen's and Bukkholm's experimental data. Their finding showed similar concentrations of magnesium retention and calcium production, however, slightly more calcium was produced. The retained magnesium was associated with magnesium precipitation in the chalk core and dissolution of calcite. Higher chemical reaction was observed at lower injection rate, flow rate ranging from 0.25 PV/day to 16 PV/day. In addition, their experimental data were used to propose a new way to match reaction kinetics of calcite and magnesite mineral reactions.

Korsnes and Madland (2017) observed that injecting strontium- and barium-based brines at 130 °C in outcropped Mons chalk led to a strain reduction. After 420 days of creep with magnesium brine, strontium-based brine was injected, and then barium before a complete stop. However, the chemical interaction of strontium- and barium ions with the outcrop chalk showed similar trends as observed with magnesium. It was discussed the if the formation of secondary minerals, larger than calcium carbonate, would reduce compaction rates by increasing the solid volume and/or by creating increased intergranular friction between grains.

1.1. Objective

This work aims to run systematic experimental tests with strontium- and barium-based brines in chalk at reservoir temperature relevant to the Ekofisk field. This experimental study will investigate the reaction kinetics of strontium- and barium-based brines on Mons chalk outcrops. More specifically how rate dependency affects steady state perception of strontium and barium in chalk. Upon flooding reactive brines in chalk, effluent concentrations will gradually reach a

steady state and thereafter flow rate is systematically adjusted to observe how the reaction kinetics alters with the flow rate change.

Former studies have investigated the effect magnesium has on mechanical properties and how the reaction kinetics between the ion and chalk are affected by injection rate. Those studies showed that the interaction between magnesium and chalk is rate-dependent and makes the rock mechanically weaker (Nermoen et al., 2015; Sachdeva et al., 2019; 2020). Korsnes and Madland's (2017) study has shown that injecting larger divalent cations, such as strontium and barium, will strengthen the chalk. Analyses of the effluent brine show that strontium and barium ions interact with rock. However, their study did not investigate the rate effect upon injection of strontium or barium. Based on the effluent profile, the brine-rock interaction looks similar to the interaction between chalk and magnesium s substitution-like behavior. Nevertheless, will we see the same dependency rate when injecting strontium and barium? Will we see the same effluent concentrations of strontium and barium when magnesium is not initially injected?

1.2. Limitation

The dominant factor limiting data collection regarding this experimental test is time. Due to the time constraints of the MSc thesis, a time interval for flooding and collecting data had to be implemented. Inhibiting the magnitude of sampling data and depth of investigation.

2. Theory

2.1. Chemistry

This experiment focuses on the interactions with selected divalent ions (Sr^{2+}, Ba^{2+}, Mg^{2+}) and calcium (Ca^{2+}) in chalk. The chemical interaction can be interpreted as a substitution-like process, with dissolution of Ca^{2+} and precipitation of Sr^{2+}, Ba^{2+}, and Mg^{2+} bearing carbonates (CO_3^{2-}). The interactions can be expressed as follows:

$$CaCO_{3\,(s)} + Sr^{2+}_{(aq)} \rightleftharpoons SrCO_{3\,(s)} + Ca^{2+}_{(aq)}$$

$$CaCO_{3\,(s)} + Ba^{2+}_{(aq)} \rightleftharpoons BaCO_{3\,(s)} + Ca^{2+}_{(aq)}$$

$$CaCO_{3\,(s)} + Mg^{2+}_{(aq)} \rightleftharpoons MgCO_{3\,(s)} + Ca^{2+}_{(aq)}$$

Observing the equations above sodium and chloride are excluded. Even though sodium and chloride ions were mixed in the brine, they will not be expected to interact with the chemical prosses. Thus, equal concentrations of sodium and chloride ions are expected in the effluent samples and injection brine.

2.1.1. Equilibrium constant

In 1864, Guldberg and Waage suggested their law of mass action (LMA). Essentially a statement of matter, meaning matter is not created nor destroyed, and its quantity is the same for the reactant and product. Guldberg-Waage states:

$$aA + bB \rightleftharpoons dD + eE \qquad 2.1$$

Where A, B, D, and E are chemical species involved and a, b, d, and e are their coefficients in the balanced chemical equation. The state of the reactions shown above can be described in terms of equilibrium. The equilibrium state does not give any information regarding the pathway or time it takes to reach equilibrium for a given temperature. Equilibrium constant expression builds on the concept of LMA (equation 2.1) and is expressed as:

$$K_c = \frac{[D]^d[E]^e}{[A]^a[B]^b} \quad 2.2$$

Equation 2.2 is called equilibrium-constant expression, where brackets [i] denotes molar concentration, K_c is the equilibrium constant (dimensionless). The equilibrium constant relates to the kinetics of a reaction, thermodynamics and derives from thermodynamic measurements in terms of activities. However, reference the reader to Brown et al. (2012) chapter 19 and Brezonik & Arnold (2011) chapter 4 for further reading regarding thermodynamics and thermodynamic measurements.

Heterogeneous equilibria are when substances in equilibrium are in different phases, e.g. rock-fluid interaction in this experiment. The concentration of a solid will always be one. Thus, the equilibrium constant for equation 2.2. is written as:

$$K_c = [Ca^{2+}][CO_3^{2-}] \quad 2.3$$

The value of K_c only depends on the particular reaction and the temperature. Hence, when the balanced chemical equation for a reaction is known, we can write the equilibrium constant even if we do not know the reaction mechanism. Which means the equilibrium constant is based on stoichiometry, not the mechanism (Brown et al., 2012).

2.1.2. Charge balance

Charge balance states that the sum of positive charges equals the sum of negative charges, and any aqueous solution can be written as:

$$\sum \text{equivalent of cations} = \sum \text{equalent of anions} \quad 2.4a$$

$$n_1[C_1] + n_2[C_2] + \cdots = m_1[A_1] + m_2[A_2] + \cdots \quad 2.4b$$

Where C is the concentration of all the cations in solution, n is the magnitude of the respective cation charge, A is the concentration of all the anion charged ions, and m is the magnitude of the respective anion charge. Ideally, the net charge should be zero, but the analytical error must

be considered in complex aqueous solutions. Therefore, the charge balance error (CBE) equation can be used to express how far off the analysis are:

$$\mathrm{CBE} = \frac{\sum \text{equivalent of cations} - \sum \text{equivalent of anions}}{\sum \text{equivalent of cations} + \sum \text{equivalent of anions}} \times 100 \qquad 2.5$$

CBE can be positive or negative, as a positive CBE indicate a higher concentration of cations, and conversely, a negative CBE indicates a higher concentration of anions. Acceptable CBE calculations are considered to be below 5 % (Kamel et al., 2011).

2.1.3. Carbonate dissolution

The carbonic acid system is fundamental for understanding the dissolution of carbonate. If we have a beaker filled with water, gaseous carbon dioxide (CO_2) will become aqueous in solution and form carbonic acid (H_2CO_3).

$$\mathrm{CO_{2\,(g)}} \rightarrow \mathrm{CO_{2\,(aq)}} \qquad 2.6$$

$$\mathrm{CO_{2\,(aq)}} + \mathrm{H_2O_{(l)}} \rightarrow \mathrm{H_2CO_3} \qquad 2.7$$

Carbonic acid is capable of donating proton (H^+), therefore, decreasing the pH of the solution. If the carbonate is exposed to carbonic acid, the carbonate ion (CO_3^{2-}) from the rock matrix will react with a proton to form bicarbonate (HCO_3^-) which dissolves calcium carbonate ($CaCO_3$). Subsequently, the overall reaction can be written as:

$$\mathrm{CO_{2\,(g)}} + \mathrm{H_2O_{(l)}} + \mathrm{CaCO_{3\,(s)}} \rightarrow \mathrm{Ca^{2+}_{(aq)}} + 2\mathrm{HCO^{-}_{3\,(aq)}} \qquad 2.8$$

This reaction is fundamental for understanding the behavior of $CaCO_3$ dissolution and precipitation (Appelo & Postma 2005). Equation 2.8 shows that the magnitude of carbonate dissolution is dependent on pH.

2.2. Ion chromatography

Ion chromatography has a significant influence on the results discussed in this thesis. Therefore, it seems appropriate to explain the theory behind this machine and how the concentration of effluent samples is calculated.

Ion chromatography (IC), a liquid chromatography, is an analytical technique for separating and determining anionic and cationic analytes in various sample matrices. IC separates ions based on interactions with resin and eluent, i.e., a stationary and mobile phase. The phases differ between an anion and cation column, attracting the corresponding ions. Thus, each column can only measure the conductivity of the specific ions. Through the column, ions will move at different speeds depending on their affinity for the specific resin and separate based on ion charge and size differences. As the eluent passes through the column, ions will move through the column based on their affinity. Therefore, the weaker the affinity of the ion, the slower it will move through the column (Dalefield, 2022). An electrical conductivity detector measures the ions as they exit the column and produces a chromatogram that plots conductivity vs. time. Each ion produces a peak and an area on the plotted graph, representing the concentration of the explicit ion. Hence, standards with pre-known concentrations must be analyzed with the effluent samples to compare the area and calculate the ion concentration.

2.2.1. Ion concentration calculation

Ion concentrations calculations base its concept on linear interpolations. The area of the respected ions is related to its concentration. A larger area will resolve into higher concentrations and vice versa. The area of standard with pre-known concentrations are used to compare the area of each ion contained in the effluent samples. Hence, the standard must contain ion composition as the effluent samples. Theoretically, the relationship between the area of the respective ion and the ion's concentration equals a constant, see equation 2.9a. However, when conducting experimental testing, uncertainties have to be considered. These uncertainties can be the accuracy of the IC machine or human error, this will be further explained in section 5.4. Hence, the pre-known standard concentrations should be mixed with similar concentrations of the effluent samples to calculate precise ion concentrations.

$$\left[\frac{A_{std}}{C_{std}}\right]_i = \left[\frac{A_{eff}}{C_{eff}}\right]_i = \text{constant} \qquad 2.9a$$

Where i is the respective ion in focus (e.g., Na^+, Cl^-, Ca^{2+}, etc.), A_{std} is the area of standard solution, C_{std} is the concentration of the standard solution, A_{eff} is the area of the effluent sample, and C_{eff} is the concentration of the effluent sample. By rearranging equation 2.9a, we are left with one unknown.

$$[C_{eff}]_i = \left[\frac{A_{eff}}{A_{std}} C_{std}\right]_i \qquad 2.9b$$

For this experimental analysis, three standards were used to calculate the ion concentrations of the effluent samples. Each standard calculates a value of ion concentration from equation 2.9b, and then compared for credibility. If all standards calculated similar effluent ion concentrations, an average value is taken and used in the data analysis. The effluent analysis was re-run if the calculated concentrations show high uncertainty, see section 5.4.

3. Experimental setup

This experiment was conducted to understand better flow rate dependency and reaction kinetics between three divalent cations flooded through chalk outcrops. As reservoir cores are complex in mineralogical composition, it is reasonable to make more reliable conclusions by using pure outcrop chalk cores while studying the interaction between brine and chalk formation. In this reactive flow study, parameters such as temperature, pore- and confining pressure were constant to observe how the chemical reaction rate between brine composition and chalk core is dependent on flow rate.

3.1. Rock and fluids

Outcrop chalk cores from Mons Belgium, specifically Harmignies quarry, were used to conduct four experiments. The outcrops originate from the Campanian age with a high carbonate content of 99.7 weight % and a specific surface area of 1.8 m^2/g (Megawati et al., 2015). The cores were drilled out from a chalk block using a coring drill bit. After drilling, the cores were shaped to the desired diameter of ~38 mm using a turning lathe. Some cores had to be polished on either inlet or outlet, due to small cracks, to create a smooth and parallel end surface. Thus, core lengths vary from 73.0 to 75.7 mm.

After measuring the core's diameter and length, the cores were placed in a heat chamber for at least 24 hours to obtain accurate dry mass measurements. After that, the saturated mass was acquired by placing the test cup and core in a vacuum chamber, see figure 3.1. The chamber was then depressurized using a vacuum pump and a gauge attached to the chamber. When the pump reached zero pressure, the core was saturated with distilled water (DW) until the core was fully submerged. Before obtaining the saturated mass, water film surrounding the core was eliminated to acquire accurate measurements. Porosity was calculated using dry and saturated mass to determine pore volume (V_p) and calculated bulk volume (V_b), shown in equation 3.1.

$$\varphi = \frac{V_p}{V_b} = \frac{\frac{(W_s - W_d)}{\rho_w}}{\left(\frac{D}{2}\right)^2 \times \pi \times L} \quad 3.1$$

Where φ is the porosity, V_p is the pore volume, V_b is the bulk volume, W_s is the saturated weight of the core, W_d is the dry weight of the core, ρ_w is distilled water density, D is the core diameter, and L is the core length.

Figure 3.1: Vaccum chamber used to saturate the cores

Table 3.1: Core properties of the outcropped chalk used in the flooding experiments

Core ID	Diameter [mm]	Length [mm]	Dry mass [g]	Saturated mass [g]	Porosity [%]	1 PV/day [ml/min]
ME8	37.99	75.04	128.98	166.40	43.99	0.026
ME10	38.00	74.04	126.92	163.95	44.10	0.025
ME18	38.02	73.27	125.28	162.15	44.32	0.025
ME22	38.02	75.65	130.25	167.95	43.90	0.026

All brines used in this study were mixed to a 0.12 mole per liter (mol/L) concentration. The use of small concentrations was because barium chloride was used in two of the brines. Barium chloride is toxic if swallowed, harmful in inhalation, and can cause irritation, nausea, headache,

and eye-, skin-, and mucous membrane irritant (Barium chloride dihydrate, 2022). Therefore, a decision was made to use a lower concentration than in the previous experiments with magnesium chloride ($MgCl_2$) (Andersen et al., 2022). Lastly, all brines contained sodium chloride (NaCl) to create similar ionic strength as seawater, 0.657 mol/L.

ME22 and ME18 were flooded with 0.12 mol/L strontium chloride ($SrCl_2$) and barium chloride ($BaCl_2$), respectively. ME22 was prepared by mixing strontium chloride hexahydrate ($SrCl_2$ x $6H_2O$) and NaCl in DW to its desired concentration, and ME18 was prepared with barium chloride anhydrous ($BaCl_2$ x $2H_2O$) and NaCl. Both cores were flooded for five weeks to collect data to decide the brine composition used for ME10 and ME8. Eventually, it was decided to flood ME10 and ME8 with a mixture of 0.06 mol/L $MgCl_2$ and $SrCl_2$, and 0.06 mol/L $BaCl_2$ and $SrCl_2$, respectively. The magnesium chloride used in ME10 was prepared using $MgCl_2$ x $6H_20$ up to 0.06 mol/L. The full brine composition used in the cores can be found in table 3.2.

Table 3.2: Ion composition of all injection brines used on outcrop chalk

Core ID	Cl^- [mol/L]	Na^+ [mol/L]	Sr^{2+} [mol/L]	Ba^{2+} [mol/L]	Mg^{2+} [mol/L]
ME8	0.537	0.297	0.060	0.060	0.000
ME10	0.537	0.297	0.060	0.000	0.060
ME18	0.537	0.297	0.000	0.120	0.000
ME22	0.537	0.297	0.120	0.000	0.000

The brine composition of each desired core did not change throughout the experiment. The brine was flooded till nearly empty and replaced with a brine of the same ion concentration. All brines used for this experiment were, after mixing, filtered with a 0.65 μm MCE membrane of type MF-Millipore to remove any potential particles. Lastly, pH measurements were performed on all brine mixtures to secure consistency, the pH ranged between 5.46 and 5.94.

3.2. Test cell assembly procedure

The experiments were conducted using a hydraulically operated triaxial cell. Some preparations had to be done in order to assemble the triaxial cell. The brine tank was cleaned and filled with its chosen brine composition. The flowlines were flushed with DW to eliminate any remaining salt in tubing from previous experiments and flushed with brine. After these preparations were done, the assembling of the triaxial cell could begin.

Firstly, a distribution plate was placed on the inlet and outlet of the Mons core, held together by a gasket. The core with distribution plate was then placed on an inlet socket, and a shrinking sleeve was fitted around the core to isolate the core material from the confining chamber, see figure 3.2a and 3.2b. A heat pistol was used to warm up the shrinking sleeve to fit the sleeve around the core properly. An extensometer (measures change in core diameter) was fitted on the core before the top socket was assembled. Then the top socket was assembled to the core outlet (see figure 3.2c) before mounting the confining chamber with a heat jacket. The confining chamber was filled with marcol 82 to control the confining pressure. The cell top was then mounted and bolted to complete the triaxial cell, and a linear variable differential transformer (LVDT) was assembled on the piston on the cell top. The LVDT measures the core displacement along the height axis. The triaxial cell was complete (see figure 3.3) and the flowline and pressure system could be mobilized.

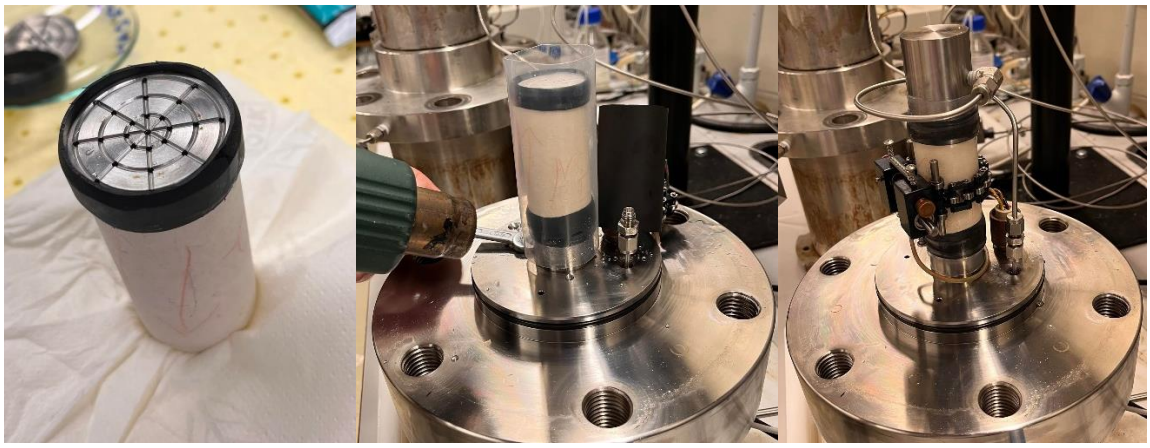

(a) *(b)* *(c)*

Figure 3.2: (a) Test core with distribution plate and gasket, (b) core mounted on inlet socket and a heating pistol used to on shrinking sleeve, (c) Outlet and extensomenter mounted on core

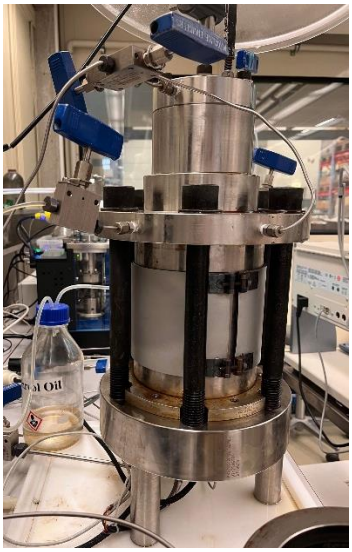

Figure 3.3: Triaxial cell set-up after completion

The pressure system consists of three pumps, axial- (#2), confining-(#3), and brine pump (#6), connected by a flowline system to the triaxial cell (#4), shown in figure 3.4. The two pumps controlling axial and confining pressure were either Quizix QX-series or Vindum VP-series. Quizix QX-series and Vindum VP-series are run by two independently controlled motor-driven pistons and can apply constant flow rate for pressure buildup or withhold constant pressure. The two pumps are supplied by an oil tank (#1) containing marcol 82 and connected to a flowline to confining chamber and axial piston chamber. Pressure gauges (#8d and #8c) are connected to axial and confining pressure flowlines and give the ability to log pressure. The flow rate was operated by a Gilson 307 pump (#6) and fluid was supplied by a DW tank (#5) which flows DW at a constant rate to the brine tank (#7). A bypass through the brine tank was installed. However, this is only used during pre- and post-flush of the flowline system before and after the experiment, thus, closed during experimental testing. The brine tank consists of two chambers, a brine chamber and a DW chamber (brine being marked by dark blue color and DW being light blue color in figure 3.4), and a subdivider. The subdivider has a seal ring around to secure the brine, and DW does not mix. Thus, the brine is contained in a closed system throughout the flooding. DW flows from Gilson 307 pump to the DW chamber in the brine tank, pushing on the subdivider and displacing brine out of the brine chamber. Brine is then flooded to the inlet of the triaxial cell and a differential pressure gauge (#8b). The differential pressure gauge measures the pressure difference between inlet and outlet. As brine is flooded through the core towards the outlet, the predetermined pore pressure is set by a back pressure regulator (#11) and

gas regulator (#10). A pore pressure gauge (#8a) is also connected to the outlet for logging. The effluent water passing the back pressure regulator could then be sampled (#12).

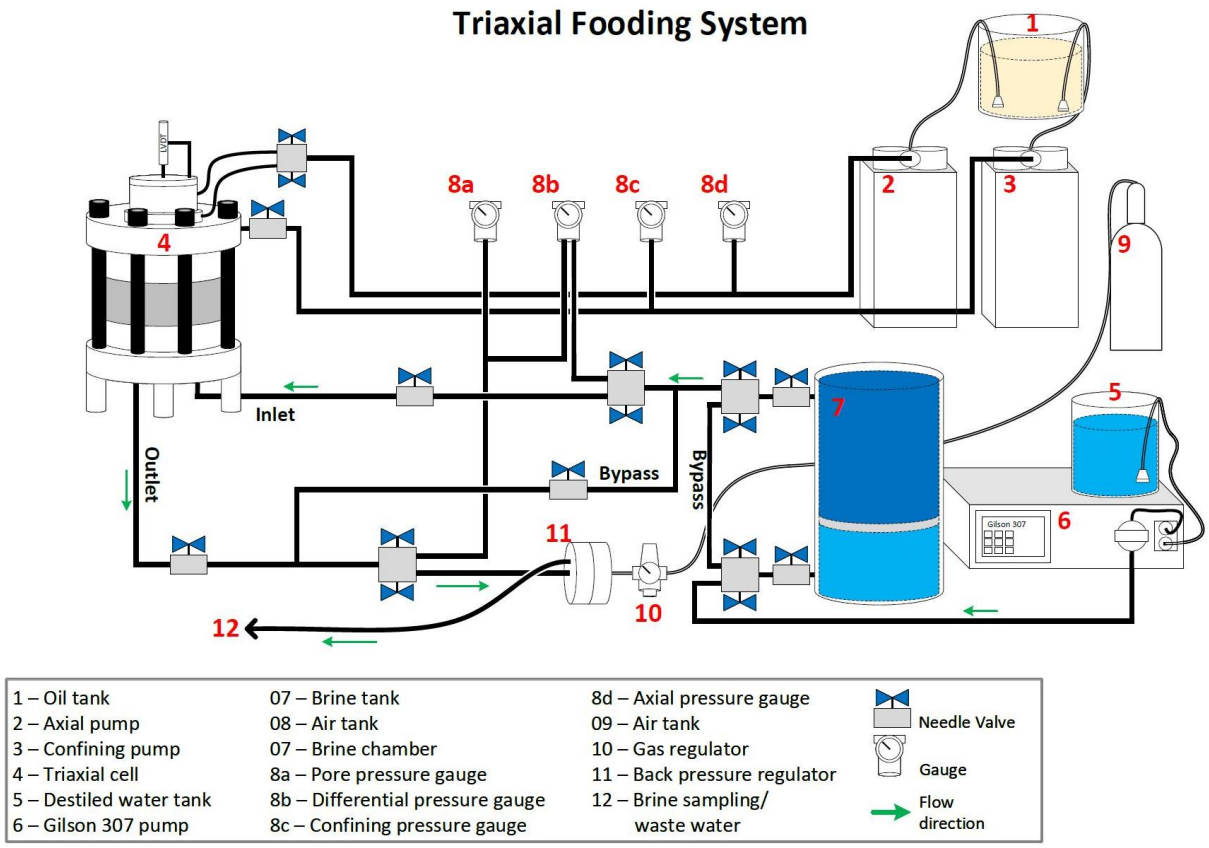

Figure 3.4: Layout of the triaxial flooding system

3.3. Experimental test condition

A leak test was conducted to ensure a correct setup was compiled with the triaxial cell assembled and connected to the flowline system. The leak test was performed by increasing confining pressure to 0.5 mega pascal (MPa) and landing the piston on the core (controlling the axial pressure and axial deformation). Landing the axial piston on the core was observed by LVDT and axial pressure log. Axial pressure is constant when the piston is moving down towards the core but increases when the piston meets the core, and the axial pressure pump is turned off. Axial pressure is then set to a pressure 0.3 MPa higher than the pressure measured when moving

the piston down to ensure that the piston follows the movement of the core. After an acceptable leak test, further proceeding could continue to achieve core conditions.

The core conditions used in this experimental study are the same as in Andersen et al. (2022). All four core experiments encountered the same pore and confining pressure 0.7 MPa and 2.0 MPa, respectively. The temperature was set to 130 degrees Celsius for all cores and is the expected reservoir temperature at Ekofisk.

Core conditions were achieved by increasing pore and confining pressures simultaneously from zero to 0.7 MPa and from 0.5 MPa to 1.2 MPa, respectively. Pore pressure buildup was performed by opening the by-pass valve connecting inlet and outlet flow tubing. Increasing the gas pressure for the back pressure regulator system up to 0.7 MPa, and then start brine injection. After achieving 0.7 MPa pore pressure and 1.2 MPa confining pressure, the injection rate was set to one pore volume per day, before the temperature increase could be conducted. The temperature increase was managed by the heating jacket mounted on the outside the triaxial cell in combination with a pt-100 sensor inside the confining chamber to log the internal temperature. Due to the expansion of marcol 82 oil inside the confining chamber when temperature increase was initiated, a back pressure regulator was connected to the confining chamber valve to withhold stable confining pressure till 130 °C. Lastly, confining pressure was increased from 1.2 to 2.0 MPa.

3.4. Flooding and sampling procedures

After a complete setup of the experiment, with core conditions achieved, core flooding and sampling could begin. ME22 and ME18, the first cores to start collecting data, had similar predetermined flooding procedures. ME10 and ME8 had a divergent program as they were initiated later. However, all cores were initiated with a flow rate of approximately one pore volume per day (PV/day), 0.026 ml/min.

ME22 and ME18 started with a flow rate of 1 PV/day followed by consecutive flow rates of 2 PV/day, 4 PV/day, and 8 PV/day. 8 PV/day was the maximum flow rate achieved during the experiment since higher flow rates could result in a cooling effect on the core. After attaining a steady state with a maximum flow rate for ME22 and ME18, the flow rate was decreased to 1

PV/day to observe if equivalent effluent concentrations could be obtained as in the first flooding phase. At the end of the experiment the flow rate was decreased to 0.5 PV/day, before it was increased back to 1 PV/day. At the end of experimental testing with ME18 and ME22, the cores were flushed with DW to wash remaining brine inside the cores and to obtain new saturated- and dry mass measurements. Also, a collective of effluent samples was continued throughout DW flooding to ensure the cores had been properly flushed.

As ME10 and ME8 had a shorter experimental duration, the flow rate was, after 1 PV/day, increased only to 4 PV/day before it was decreased to 1 PV/day. Lastly, the flow rate was then decreased to 0.5 PV/day before data collection had to be stopped due to time limitations. A complete overview of all flooding sequences can be found in table 3.3.

Table 3.3: Flooding sequences used for the specified core ID

Core ID	Flooding 1 (PV/day)	Flooding 2 (PV/day)	Flooding 3 (PV/day)	Flooding 4 (PV/day)	Flooding 5 (PV/day)	Flooding 6 (PV/day)
ME8	1	4	1	0.5	-	-
ME10	1	4	1	0.5	-	-
ME18	1	2	4	8	1	0.5
ME22	1	2	4	8	1	0.5

Effluent samples were collected and analyzed to determine if a steady state had been reached. Each sample was collected by a sampling machine (GX-271 Liquid Handler) into a vial glass with approximately 5 ml of effluent brine. Effluent sampling intervals were dependent on flow rate and stage of the flooding sequence. Rapid sampling was conducted at the initial stage of every flow rate transition as reactivity was expected to be higher. Thereafter, the duration between each sampling increased. Throughout the experiments, high-frequent sampling was considered 0.5 – 1 PV injected between each sampling, and longer intervals were considered 1-3 PV injected. Therefore, sampling was conducted continuously at a higher flow rate, e.g., 8 PV/day. After sampling, the vials were capped to avoid evaporation and stored in a refrigerator. Furthermore, after multiple effluent samples were collected, samples were then taken to ion chromatographic analysis to detect any change in ion concentration.

3.5. Ion chromatography analysis

The effluent samples were analyzed using an ion chromatograph (IC). Precisely for this experimental study, a Dionex Ion Chromatography System (ICS)-5000. Every IC analysis was conducted with sampled effluent brines and three different standards. Standards used were synthetic seawater (SSW), calcium chloride ($CaCl_2$) mixture with divalent ions from the original injection brine, and a sample of the original brine used for the respective core. Standards were analyzed to calculate the effluent concentration and explained in section 2.2.1.

An ion chromatography machine is susceptible and requires some preparations before the analysis of the effluent samples can be managed. Samples had to be taken to a liquid handling machine, where the samples were diluted with nano pure water . Nano pure water is treated water with all ions removed to remove interference with IC analysis. The liquid handling machine collected a specimen from the effluent sample vial and diluted the specimen 1000x in another clean vial, see figure 3.5. The diluted brine was then transferred using a syringe and 0.65-micron filter, into a smaller plastic vial fit for the IC machine. The filter is used to remove contamination from samples and protect the IC instruments. This procedure had to be repeated for all samples analyzed by the IC.

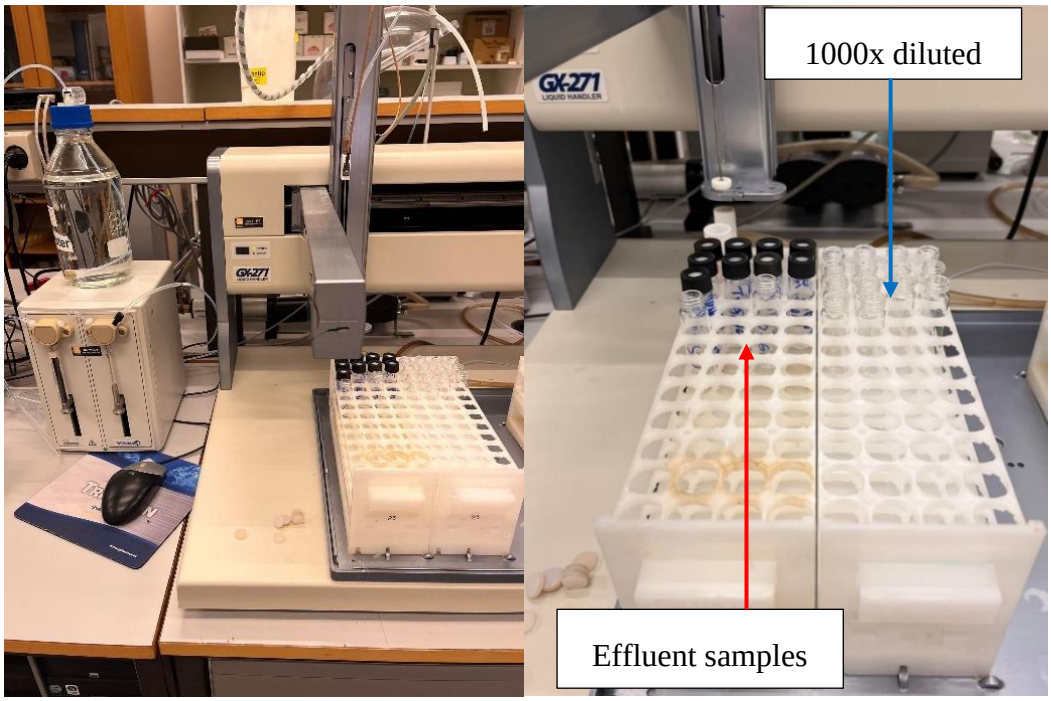

Figure 3.5: Liquid handling machine and effluent samples ready to be diluted

3.6. Disassembling the cores

After completing the test, ME18 and ME22 were disassembled from the triaxial cell. New saturated- and dry mass measurements of the cores were conducted after testing, followed by measuring new core length and diameter to calculate the bulk volume.

Immediately after disassembling the core from the triaxial cell, the core was moved to a scale to obtain a new saturated mass. Edges of the core were dried off with the same procedure as obtaining saturated mass before the experiment, section 3.1. Moreover, crumbled core pieces were collected and measured with the core to ensure correct saturated and dry mass. Then saturated mass was measured until constant measurements were attained. Afterward, the core was put in a heat chamber to obtain the dry mass and measured until constant measurements were attained. Thereafter, the core was taken to a Vinci PoroPerm to determine its physical properties, porosity, density, and pore volume. PoroPerm is a steady-state gas porosity meter and determines the porosity from an isothermal nitrogen expansion and the application of Boyles law and Charles law. It should be acknowledged that PoroPerm was not used to verify the physical properties of the cores before conducting reactive flooding but determined from saturated- and dry mass measurements explained in section 3.1.

After obtaining new determined physical properties of the core, new bulk density was calculated using new dry mass. Further action was to cut the core into slices to determine the matrix density distribution from inlet towards outlet. A central cut along the height axis was conducted dividing the core in two half's, and subdividing it into left and right side. The left side was further cut in two, dividing the cores' inlet (L_1) and outlet (L_2). The right side was cut into several smaller pieces to conduct an scanning electron microscope analysis of the inlet and outlet. The right side of ME18 was cut into five pieces, and the right side of ME22 was cut into three pieces, figure 3.6.

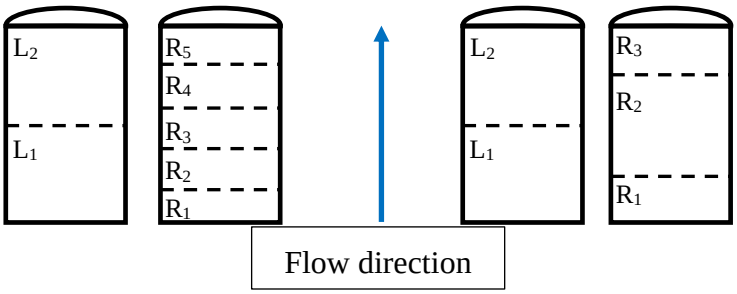

Figure 3.6: Representative drawing of cuts on ME18 (left) and ME22 (right) core, respectively

Lastly, a scanning electron microscope (SEM) was used on the core pieces to analyze how reactive flooding affected the mineralogical composition of the core. SEM uses a focused beam of high-energy electrons to generate signals at the surface of a solid (Swapp, 2017). Chemical composition, the orientation of material, and crystalline structure are some of the properties that can be reviled with a SEM. SEM is also capable of conducting qualitatively point analysis to determine the sample's chemical composition. 2-dimensional images can be captured with magnification up to 30,000-20,000X of the sampled specimen.

4. Results

The results in this study are presented in the order of longest flooding duration to the shortest. Concentrations are presented as negative and positive values. Negative concentrations are the divalent brine ions retained inside the core, and positive concentrations are produced calcium ions. Lastly, 0.0 injection days and PV injected are defined as the first collected effluent sample.

4.1. ME22 results

ME22 was flooded for 111.6 days with 0.12 mol/L $SrCl_2$ brine, and 161.0 PVs were injected. 104 effluent samples were collected and analyzed to determine the reaction kinetics of strontium on chalk. After flooding 161.0 PVs of $SrCl_2$ brine, DW flooding was initiated to remove salt from the core. Figure 4.1 presents an overview of analyzed effluent concentrations plotted against injection time in days. The expected total effluent concentration of calcium and strontium (purple data/line) should equal the original injected strontium concentration, 0.12 mol/L. The purple data/line in the figure is presented to the reader to show deviation in predicted concentrations and where the uncertainties in the data are, e.g., observe the purple data/line upon changing flow rate from 8 PV/day to 1 PV/day. The measured effluent concentration of strontium minus the injected strontium concentration and calcium concentration are plotted against pore volumes injected in figure 4.2.

Original sodium and chloride concentrations were obtained after 0.7 PV from the first effluent sample was collected. Initially, rapid calcium gain and strontium loss were detected until 9.8 PVs were injected. As flooding progressed beyond 9.8 PVs, concentration levels gradually started to stabilize towards a steady state, and after 20.8 PVs, the changes in concentrations were minimal, figure 4.2. An average from the six last data points during the 1 PV/day phase was calculated and gave calcium gain and strontium of 0.0682 and -0.0687 mol/L, respectively.

The flow rate was increased to 2 PV/day after 32.8 PVs were injected, figure 4.2. A slight decrease in retained strontium concentration was observed, and produced calcium concentration

decreased at a similar rate. Shortly after increasing the flow rate, concentration levels reached a plateau, and insignificant changes were observed. Increasing flow rate further from 2 PV/day to 4 PV/day and after that 8 PV/day gave similar trends. The difference in average retained strontium concentration with 1 PV/day and 8 PV/day was less than 7 %. The average concentration of each flooding sequence is presented in table 4.1.

The second phase of flooding with 1 PV/day, after 121.2 PVs were injected, gave similar results as the first flooding phase of 1 PV/day. Subsequently, flooding with 0.5 PV/day gave the highest concentrations of calcium gain. However, strontium concentrations were unchanged compared previous 1 PV/day flooding, see table 4.1. After reducing the flow rate to 0.5 PV/day, a drop in effluent strontium concentration was analyzed, thus, increasing strontium retention. Observing total effluent strontium and calcium concentrations (purple data/line), figure 4.1, shows a deviation from the predicted 0.12 mol/L between 77 and 79 days. Thus, it needs to be re-analyzed to confirm highest strontium concentration was obtained for 0.5 PV/day flooding. Lastly, the flow rate was set to 1 PV/day a third time, but only four samples were collected before DW flooding was initiated. The four samples gave a decrease in both strontium loss and calcium gain, table 4.1. As the third flooding phase of 1 PV/day was only conducted for a short duration, it is assumed concentrations were not stable. However, average concentrations are presented but can be misleading as it is uncertain how the concentrations would progress if further flooding continued.

Table 4.1: Average ion concentration after each flooding sequence in ME22 (steady state not reached)*

Flow rate [PV/day]	Average Ca^{2+} gain [mol/L]	Average Sr^{2+} loss [mol/L]	Pore volumes injected interval [PVs]
1	0.0682	-0.0687	0.0 – 32.5
2	0.0671	-0.0673	32.8 – 48.4
4	0.0653	-0.0654	50.8 – 89.5
8	0.0638	-0.0641	90.0 – 114.0
1	0.0689	-0.0681	121.2 – 142.0
0.5	0.0697	-0.0682	142.5 – 155.7
1*	0.0669	-0.0665	158.3 – 161.0

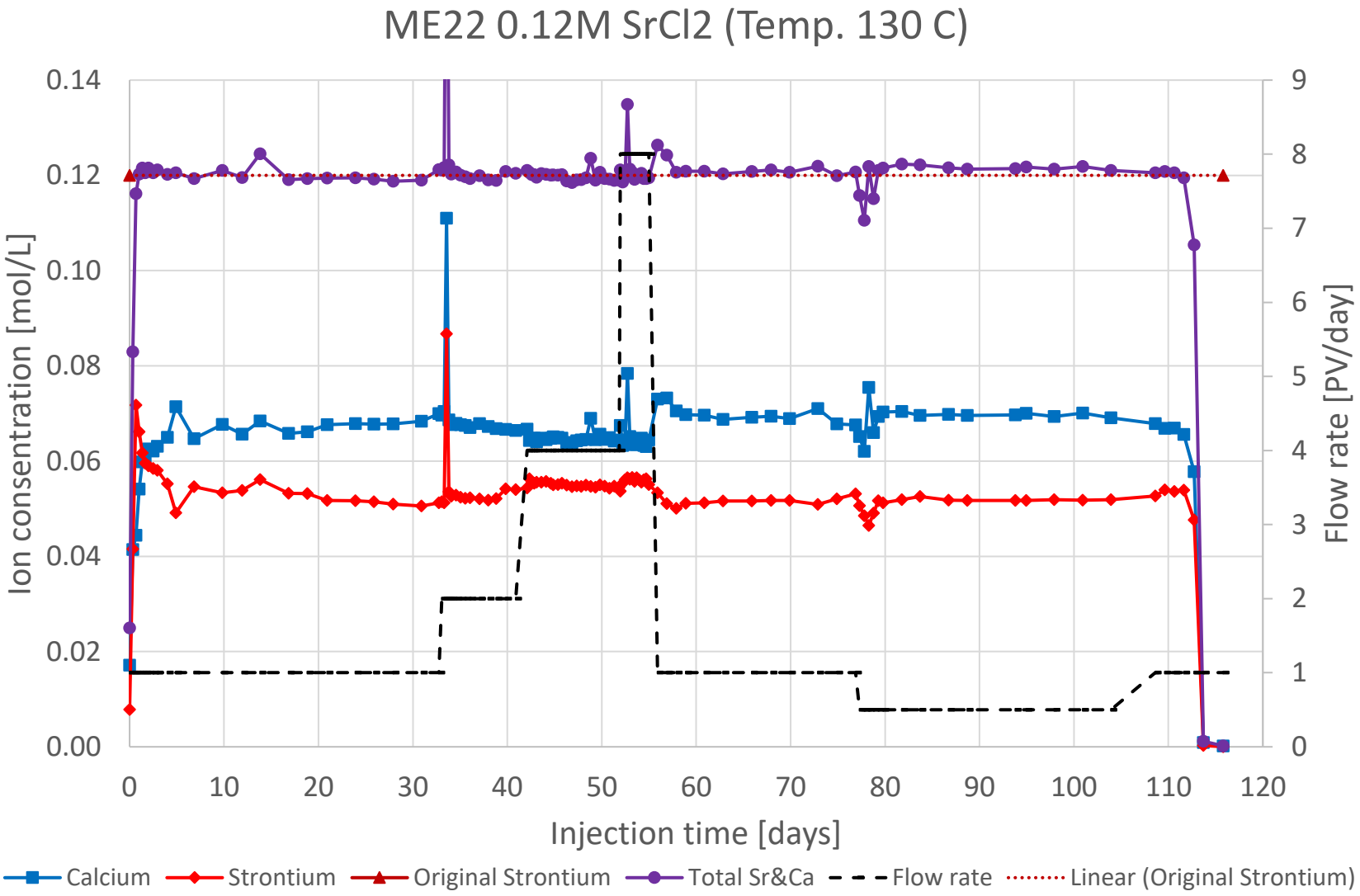

Figure 4.1: Analyzed effluent concentrations plotted against injection time in days

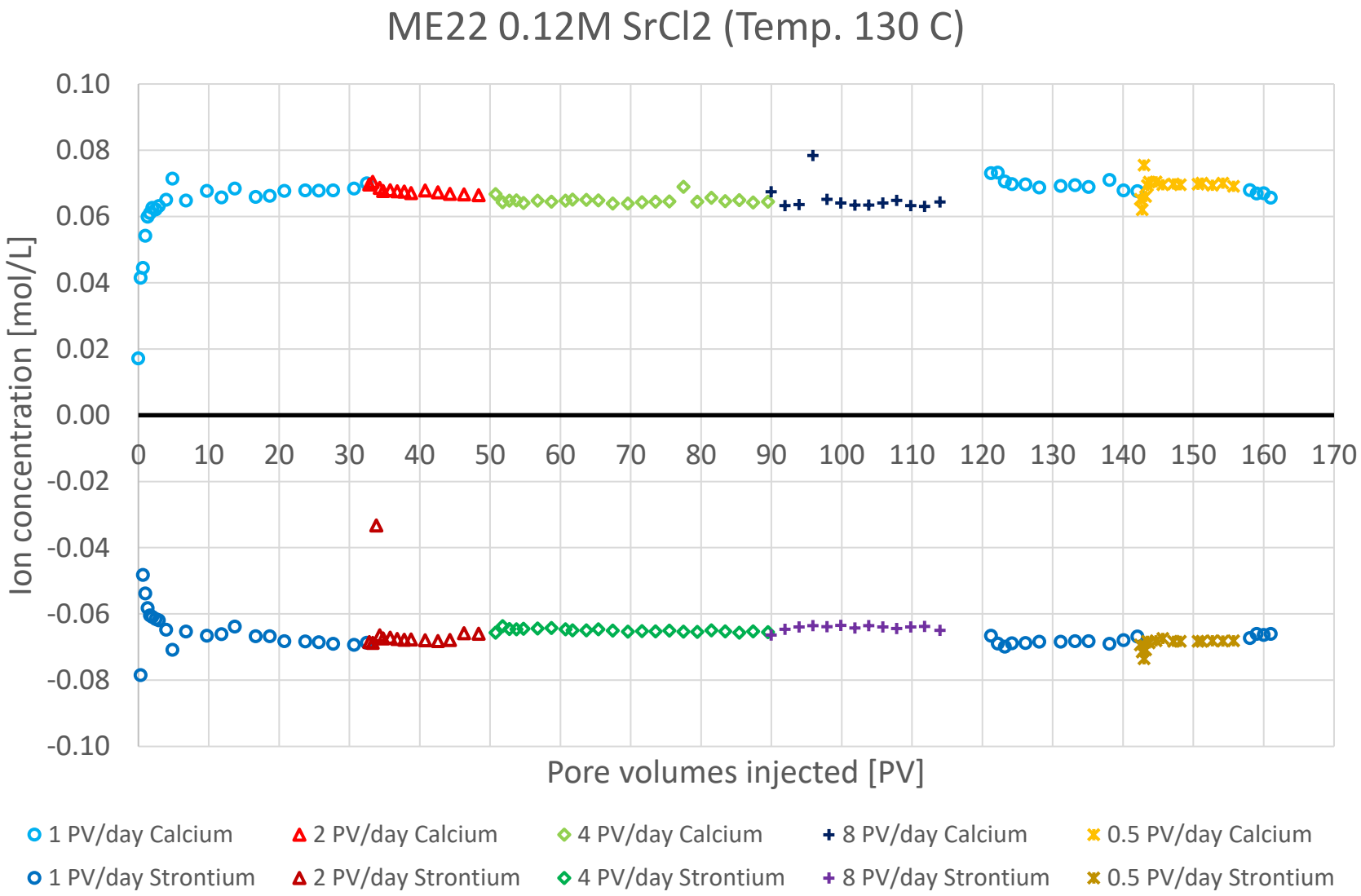

Figure 4.2: Measured effluent strontium minus the injected concentration and calcium plotted against pore volumes injected

The analyzed IC data was used to make predicted calculations of change in core mass. The molar mass of strontium is heavier than calcium. Thus, an increase in core mass was expected after injecting 5.94 liters of 0.12 mol/L $SrCl_2$. The prediction of core increase was not calculated using a simulator but simple calculations from the logged data. An average mol/L was calculated by determining the total mol lost throughout the entire flooding divided by the total brine injected:

$$\bar{C} = \frac{\sum_{i=1}^{n} |C_i| \times (V_i - V_{i-1})}{V_{tot}} \quad 4.1$$

Where $\bar{C}$ is the average concentration, $|C_i|$ is absolute strontium loss or calcium gain of i^{th} effluent sample, $V_i - V_{i-1}$ is change in injected volume between sample i and i – 1, and V_{tot} is the total brine injected. The total average calcium gain and strontium loss were 0.0669 mol/L and -0.0661 mol/L, respectively. Section 2.1.3 explained pH of brine will to some degree, dissolve chalk, thus decreasing the core mass. This was considered by using the differential of average calcium and strontium concentrations. Using the molecular weight of strontium subtracted with the molecular weight of calcium and dissolved calcium carbonate led to a calculated mass gain of 18.14 grams.

The new saturated- and dry mass of ME22 were 185.36 and 148.36 grams, respectively, leading to an increase of 18.11 grams in dry mass. The measured bulk volume after the test remained unchanged. However, measurements performed by the porosimeter showed a reduction in both porosity and pore volume, table 4.2. The average bulk density of the core was measured to have increased ~0.34 g/cm^3. An overview of the core physical properties before and after the test are presented in table 4.2.

Table 4.2: Physical properties of ME22 before and after testing

	Porosity [%]	Density [g/cm^3]	Pore Volume [cm^3]	Bulk volume [cm^3]
Before test	43.90	2.703	37.70	85.89
After test	43.26	3.042	37.15	85.89

After obtaining the measurements of the intact core, further action was to cut the core into slices to determine the matrix density distribution, see figure 3.6. Volumetric, mass, and density calculations were conducted on selected pieces cut from the core, and brine-rock reactions were observed to mostly take place at the inlet. L_1 contained a mixture of discoloration of gray and the appearance of original chalk, appendix A. The entire L_2 matrix was white and appeared to have no reaction with strontium. Lastly, the entire R_1 piece was gray and observed to have significant precipitation of strontium. R_1 obtained an estimated inlet density of 3.60 g/cm^3, table 4.3, approximately the density of pure strontium carbonate ($SrCO_3$), 3.71-3.74 g/cm^3. The density of L_2 indicated no change from the initial bulk density, see tables 4.2 and 4.3. The matrix density proved to be significantly altered at the inlet while the outlet density, L_2, remained unchanged, see table 4.3.

Table 4.3: Volumetric, mass and density calculations of cut core pieces of ME22

ME22 matrix pieces	Mass [g]	Matrix volume [cm^3]	Density [g/cm^3]
Left inlet (L_1)	42.402	12.70	3.338
Left outlet (L_2)	28.659	10.66	2.689
Right inlet (R_1)	13.344	3.71	3.596

4.2. ME18 results

ME18 flooded for 105.6 days, and 152.5 PVs were injected with 0.12 mol/L $BaCl_2$ brine. A total of 97 effluent samples were collected and analyzed, and after that, flooded with DW until the remaining brine was removed from the core before measuring new saturated and dry mass. Analyzed effluent concentrations are plotted against injection time in days in figure 4.3. Measured effluent barium concentration minus the injected barium concentration and calcium are plotted against pore volumes injected in figure 4.4. Several IC analyses of the effluent samples were done more than once due to instabilities in data from the first run of IC analysis. Further details will be explained in section 5.4, where uncertainties in data are discussed.

Original brine concentrations of sodium and chloride were obtained after 0.3 PV. After reaching original concentrations of sodium and chloride, barium appeared to give small changes in

effluent concentrations throughout flooding with 1 PV/day, figure 4.4. The average of five early data points, 0.7 – 2.0 PVs, and five late data points, 16.2 – 30.4 PVs, gave similar calcium and barium concentrations values. It should be noted that in the late data points, 16.2 – 30.4 PVs, scattered data between 19.2 PVs and 21.2 PVs were excluded in average calculations, table 4.4.

Increasing the flow rate to 2 PV/day led to a drop in concentrations, which is expected when increasing the flow rate. However, as flooding with 2 PV/day proceeded, calcium gain and retained barium increased towards comparable concentrations to 1 PV/day flooding, table 4.4. Increasing the flow rate to 4 PV/day led to a prompt drop in calcium gain and barium loss, figure 4.4. At the start of the 4 PV/day phase (59.0 PVs), measured calcium gain and barium loss were 0.0115 mol/L and -0.0114 mol/L, respectively. With time, flooding with 4 PV/day induced an increasing trend in calcium production and barium retention, figure 4.4. The increasing trend continued until the flow rate was changed at 80.7 PVs and the measured concentration of calcium gain and barium loss were 0.0140 mol/L and -0.0144 mol/L, respectively. Increasing the flow rate to 8 PV/day gave similar results as the flooding phase with 4 PV/day. Initially, calcium gain and retained barium decreased after increasing the flow rate, figure 4.4. Thereafter, an increase in produced calcium and retained barium concentrations were observed. Both flooding sequences, 4 PV/day and 8 PV/day, appeared to have an increasing calcium gain and barium loss trend, thereby failing to reach a steady state before changing the flow rate.

The flow rate decreased to 1 PV/day after flooding with 8 PV/day. An increase in produced calcium and retained barium were observed after decreasing the flow rate. The barium retention was measured 38 % higher during the second phase of 1 PV/day than in the first phase of 1 PV/day flooding, figure 4.4. Moreover, the concentrations became stable shortly after changing the flow rate. Decreasing the flow rate to 0.5 PV/day led to the highest calcium gain and barium loss, which was an expected trend. As flooding proceeded, measured concentrations were stable and reached a steady state rapidly. The barium retention change can be considered insignificant compared to the previous flooding at 1 PV/day, table 4.4.

Lastly, the flow rate was set to 1 PV/day a third time, where three effluent samples were analyzed before DW flooding was initiated. Even though flooding with 1 PV/day did not achieve a steady state, due to the short flooding durations, the analyzed data occurred to alter towards similar data as in the second flooding phase with 1 PV/day. Looking at figure 4.4, both calcium

gain and barium loss show an increasing trend throughout all flooding sequences, excluding the third flooding phase with 1 PV/day, which indicated a decreasing trend. An overview of average calcium and barium loss is presented in table 4.4.

Table 4.4: Average ion concentration after each flooding sequence in ME18 (steady state not reached)*

Flow rate [PV/day]	Average Ca^{2+} gain [mol/L]	Average Ba^{2+} loss [mol/L]	Pore volumes injected interval [PVs]
1	0.0123	-0.0122	0.0 – 30.4
2	0.0125	-0.0119	30.5 – 52.5
4*	0.0139	-0.0141	52.9 – 80.7
8*	0.0141	-0.0148	81.1 – 105.5
1	0.0187	-0.0197	112.3 – 132.7
0.5	0.0206	-0.0204	136.0 – 148.1
1*	0.0195	-0.0201	150.5 – 152.5

After injecting 152.5 PVs and 5.66 liters of $BaCl_2$ brine over 105.6 days, DW flooding was initiated. Predicted mass increase calculations were conducted for ME18 similarly to ME22. Using equation 4.1 to calculate average concentrations of produced calcium and retained barium gave almost identical values of 0.0151 mol/L. The predicted dissolved calcium carbonate used to calculate the mass change of the core was the anticipated dissolution concentration calculated from ME22 calculations. The calculated mass increase of ME18 core after testing was predicted to be 7.80 grams.

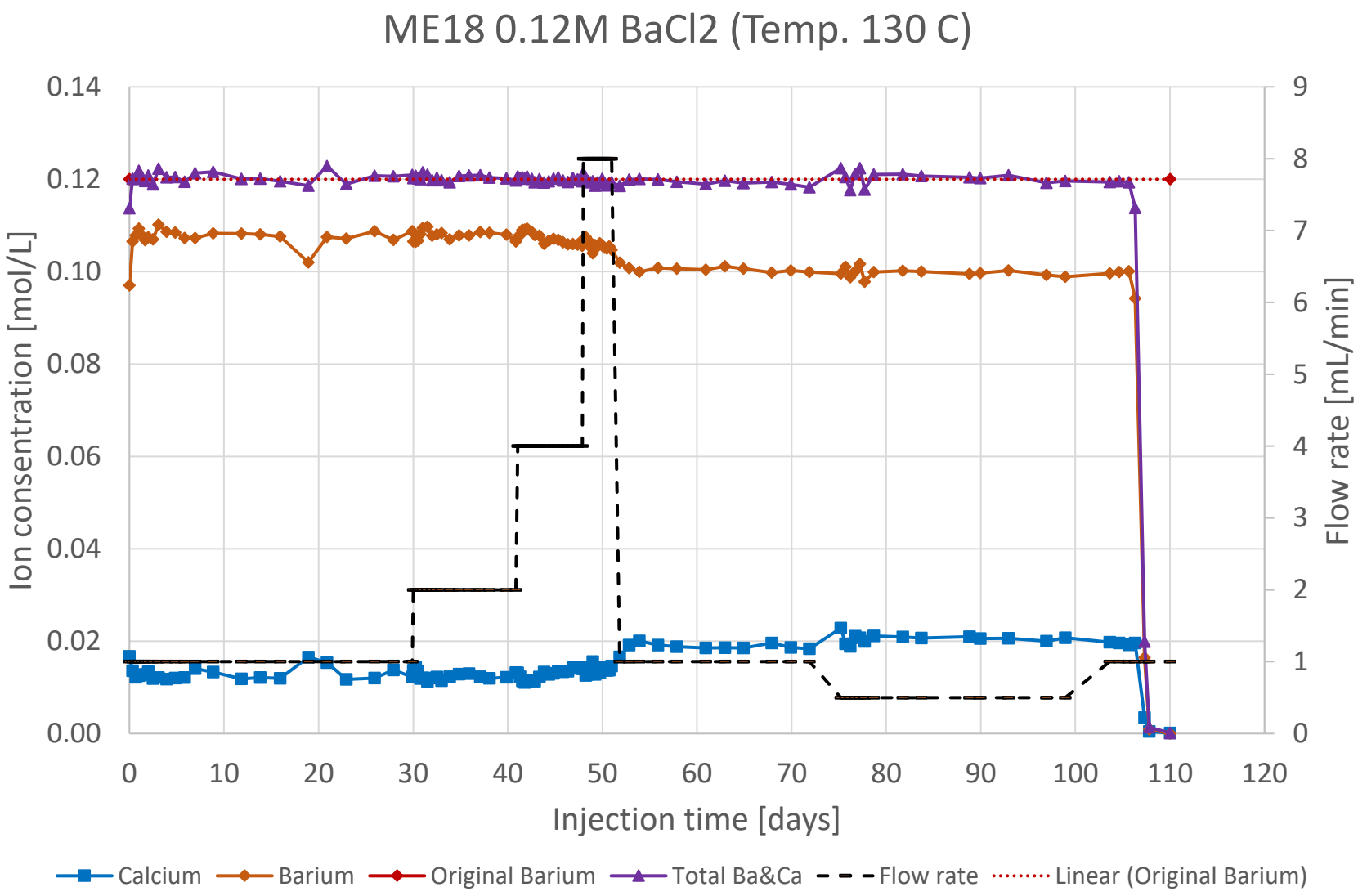

Figure 4.3: Analyzed effluent concentrations plotted against injection time in days

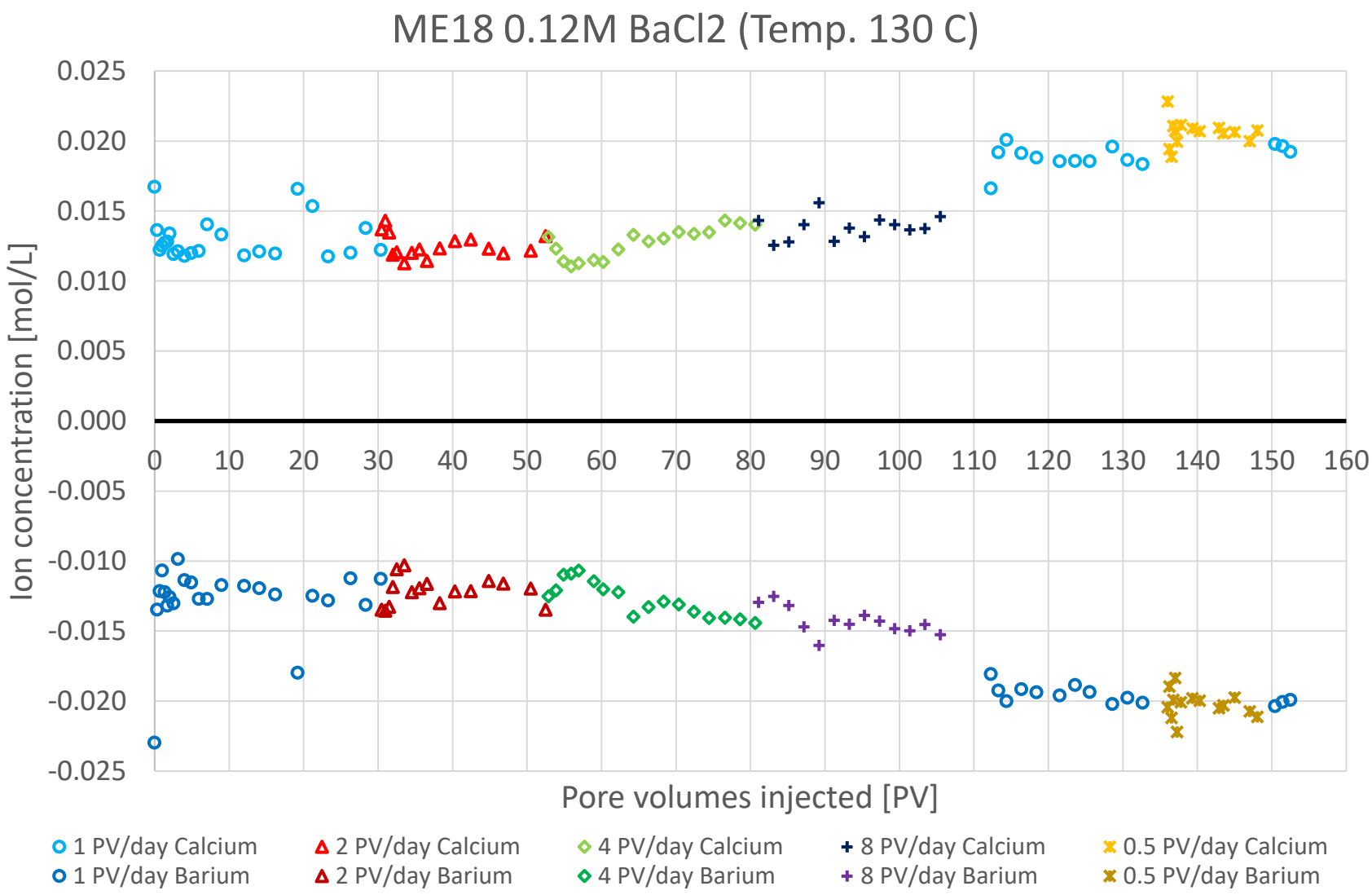

Figure 4.4: Measured effluent barium minus the injected concentration and calcium plotted against pore volumes injected

The core's new saturated- and dry mass were measured to be 168.88 grams and 132.78 grams, respectively. The change in dry mass before and after testing led to a 7.50 grams increase. The new bulk volume attained after the test was 83.21 cm^3. The core was placed into a porosimeter after obtaining the bulk volume of the core to determine porosity, density, and pore volume, table 4.5. The porosimeter measured a decrease in both porosity and pore volume and an increase in bulk density. The bulk density was measured to have increased by ~0.135 g/cm^3, less than half of the density increase obtained in ME22.

Table 4.5: Physical properties of ME18 before and after testing

	Porosity [%]	Density [g/cm^3]	Pore Volume [cm^3]	Bulk volume [cm^3]
Before test	44.32	2.705	36.87	83.18
After test	43.91	2.840	36.56	83.21

Next, the core was cut into slices to determine the density distribution. Like the ME22 core, reactions with the core and brine appeared to occur mainly at the inlet, see appendix B. Volumetric, mass, and density calculations were conducted on selected pieces cut from the core (L_1, L_2, and R_1). R_1 was calculated to obtain the highest density increase, table 4.6. This was due to R_1 having a cut focused close to the discolored front, appendix B. L_1 had a similar appearance as R_1. However, it obtained a greater volume than R_1. Thus, it had a lower density increase compared with R_1. Lastly, the calculated density of L_2 was equal to the initial bulk density before testing, table 4.6. Thereby, the matrix density calculations indicated that the reaction of barium-based brine had affected the density at the inlet of the core.

Table 4.6: Volumetric, mass and density calculations of cut core pieces of ME18

ME18 matrix pieces	Mass [g]	Volume [cm^3]	Density [g/cm^3]
Left inlet (L_1)	31.411	10.745	2.924
Left outlet (L_2)	30.404	11.255	2.701
Right inlet (R_1)	18.547	5.815	3.192

4.3. ME10 results

ME10 was flooded for 72.5 days before effluent analysis had to be stopped due to time limitations. 97.6 PVs were injected with 0.06 mol/L $MgCl_2$ and 0.06 mol/L $SrCl_2$, and 64 effluent samples collected. The experiment is still running, but new results after 72.5 days will not be added to this thesis. Effluent concentration analysis over injection time in days are provided in figure 4.5. Lastly, measured effluent magnesium and strontium concentration minus the injected original concentrations and calcium are plotted against pore volumes injected in figure 4.6.

Upon reaching original sodium and chloride concentrations, effluent calcium and strontium concentrations reached a maximum, while magnesium showed an increasing trend at 1.7 days (1.7 PVs), figure 4.5. High calcium concentration was initially detected due to a change in equilibrium when DW is replaced with brine, leading to high production of calcium. Further flooding showed a decreasing calcium production and magnesium retention trend, while strontium had an increasing trend, figure 4.6. At 19.0 PVs injected, retained magnesium reached zero. Hence, the original concentration of magnesium was measured in the effluent samples. As magnesium reaches its original concentration, calcium production and strontium retention appear to have a symmetrical trend and gradually stabilize towards a steady state, figure 4.6. Between 30.1 and 40.2 PVs, insignificant concentration changes were measured, and average concentrations could be obtained, table 4.7.

At 40.2 PVs, the flow rate was increased to 4 PV/day. The first appearance upon increasing the flow rate was a decrease in calcium production and strontium loss to 46.3 PVs, figure 4.6. Four data points of calcium gain and strontium loss between 42.3 and 46.3 PVs gave an average of 0.0229 mol/L and -0.0216 mol/L, respectively. Within the same time span, the highest magnesium retention measured was -0.0016 mol/L, before stabilizing towards the original brine concentration. As flooding continues beyond 46.3 PVs at the 4 PV/day phase, a rapid increase in strontium retention was measured, and calcium showed symmetrical results. The increasing trend of produced calcium and retained strontium until 70.4 PVs were injected, figure 4.6. Thereafter, measured concentrations stabilized, and a representative average gain/loss could be found in the data between 70.4 – 76.0 PVs, see table 4.7. Observe the positive magnesium retention in table 4.7. A positive magnesium concentration indicates magnesium is produced

but is insignificant. A reason could be inadequate standards when calculating the concentration, which will be further explained in section 5.4.

The flow rate was reduced to 1 PV/day at 76.0 PVs injected, which led to an increase in produced calcium and retained strontium, figure 4.6. Strontium retention during second phase 1 PV/day flooding was measured to have increased 35 % compared with first phase 1 PV/day flooding. Furthermore, strontium concentrations showed more stable results than in previous flooding phases. Magnesium concentrations showed no further changes, effluent concentrations being equal to its original concentration. The average magnesium, calcium, and strontium concentration from the last data points (86.3 – 93.3 PVs) during the second 1 PV/day phase are provided in table 4.7. At 93.8 PVs, the flow rate was reduced to 0.5 PV/day and led to the highest retained strontium. The highest calcium concentration was observed at the original sodium and chloride concentrations breakthrough. However, the highest calcium produced by reactive brine flooding occurred at 0.5 PV/day flooding, table 4.7.

Table 4.7: Average ion concentration after each flooding sequence in ME10

Flow rate [PV/day]	Average Mg^{2+} [mol/L]	Average Ca^{2+} [mol/L]	Average Sr^{2+} [mol/L]	Pore volumes injected interval [PVs]
1	-0.0001	0.0273	-0.0268	0.0 – 40.2
4	0.0005	0.0328	-0.0319	40.2 – 76.0
1	0.0007	0.0368	-0.0344	77.5 – 93.3
0.5	0.0010	0.0383	-0.0353	93.9 – 97.6

After the data analysis, the calculated average calcium production was 0.0022 mol/L higher than retained strontium. The result could be realistic or uncertain from the IC analysis. However, it could explain why the total concentration of effluent magnesium, calcium, and strontium (purple data/line) is above the predicted concentration of 0.12 mol/L in figure 4.5.

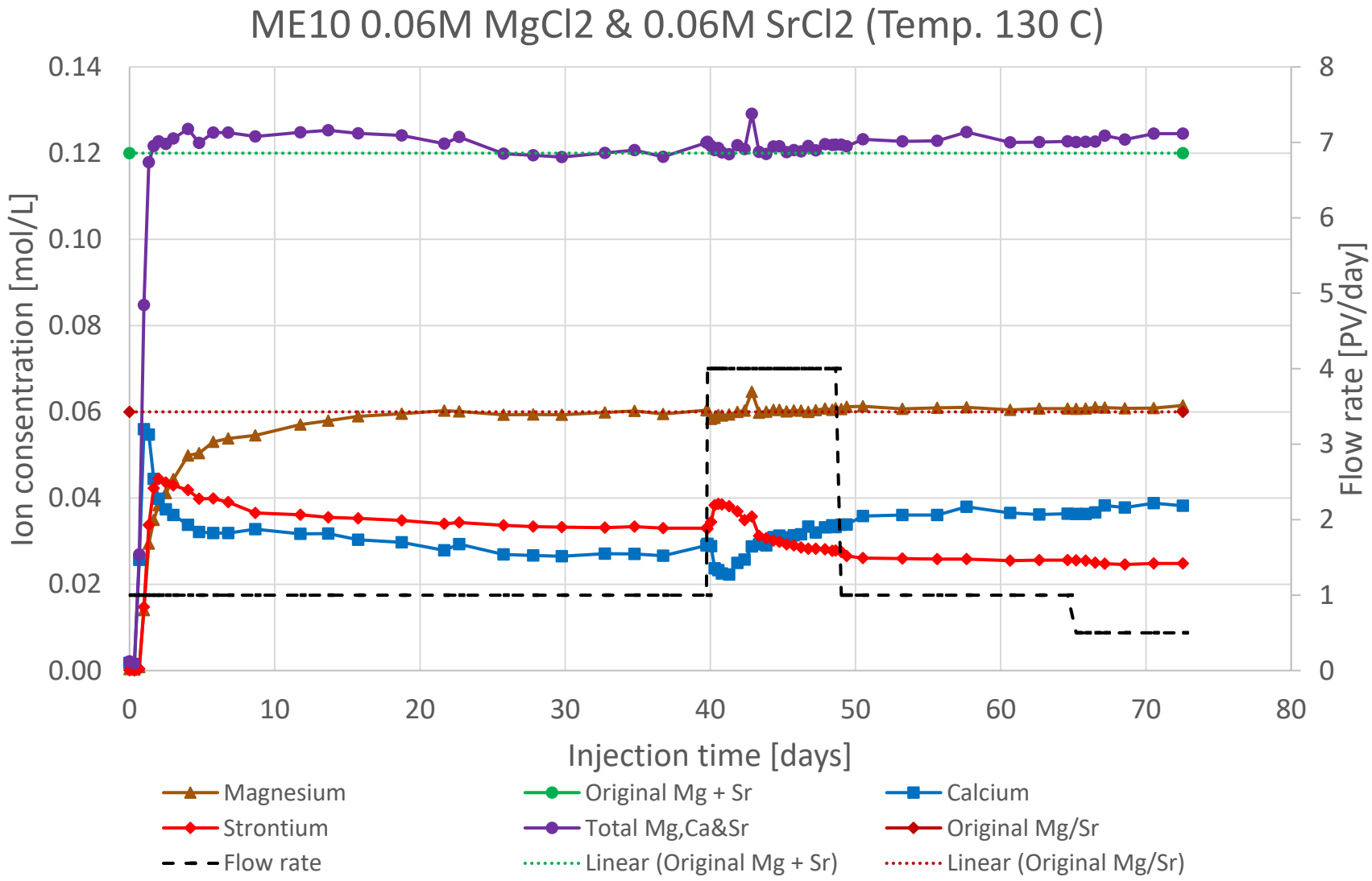

Figure 4.5: Analyzed effluent concentrations plotted against injection time in days

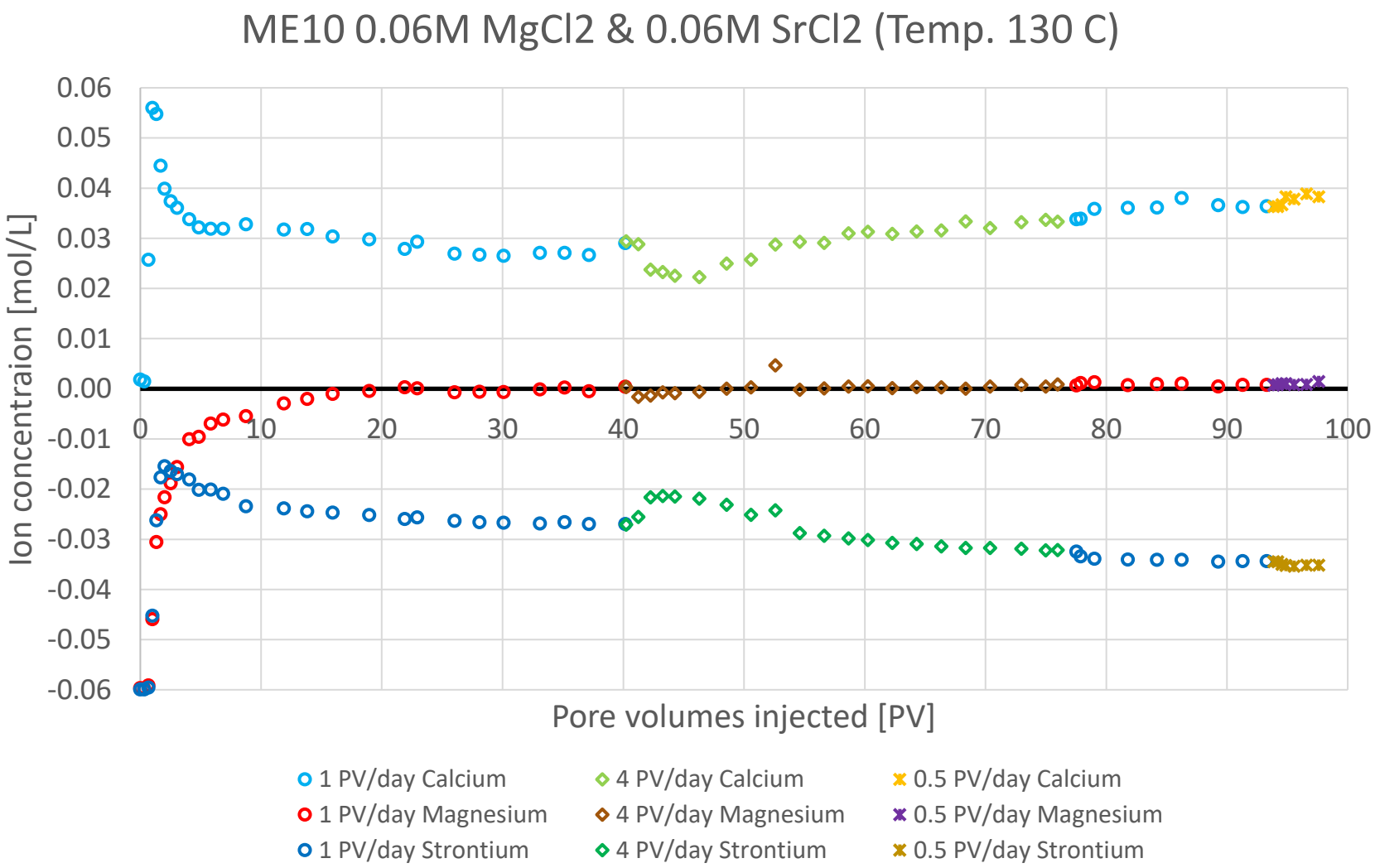

Figure 4.6: Measured magnesium and strontium minus the injected concentrations and calcium plotted against pore volumes injected

4.4. ME8 results

ME8 flooded for 70.5 days before effluent analysis was stopped for the same reason as ME10. 94.6 PVs were injected with 0.06 mol/L $SrCl_2$ and 0.06 mol/L $BaCl_2$, and 62 effluent samples were collected. A good alignment in total concentration levels is observed in figure 4.7, where concentrations of the divalent ions are plotted against injection time in days. Measured effluent concentrations of strontium and barium minus the injected original concentration and calcium are plotted against pore volumes injected in figure 4.8.

After flooding, 2.5 PVs effluent strontium concentration was at its highest with a loss of -0.0117 mol /L. Barium retention was at -0.0026 mol/L and showed stable data from early on. High calcium concentration was initially detected due to a change in equilibrium when DW is replaced with brine, leading to high production of calcium. Further flooding showed an increase in strontium loss towards 25 PVs before stabilizing towards a steady state, figure 4.7. Throughout the flooding of the first phase with 1 PV/day, barium concentrations appeared to reach steady concentrations rapidly, and insignificant changes were detected after 2.5 PVs. After flooding 27.4 PVs, all concentrations appeared to have relatively minor changes, and average concentrations were calculated: 0.0257 mol/L, -0.0218 mol/L, and 0.0027 mol/L for calcium, strontium, and barium, respectively, table 4.8.

After flooding 37.7 PVs, the flow rate was increased to 4 PV/day. Upon increasing flow rate, calcium production and strontium loss concentration decreased to an average of 0.0229 mol/L and -0.0192 mol/L, respectively, between 39.8 PV and 48.0 PV. As flooding proceeds beyond 48.0 PVs, concentrations of calcium and strontium gradually stabilize towards measured concentrations from the previous flooding, 1 PV/day, table 4.8. Moreover, barium measured a very slight increase, but it is uncertain whether the increase is due to flooding or uncertainties in the IC analysis.

During the second flooding phase of 1 PV/day, calcium gain and strontium loss increased with similar trends, thereafter providing stable concentrations of 0.0303 mol/L and -0.0263 mol/L, respectively, table 4.8. The percentage retention of strontium increased by 43.8 % during the second phase of 1 PV/day compared with the first phase. Reduction in flow rate to 0.5 PV/day led to the highest calcium production and strontium loss, excluding the initial calcium

production at breakthrough (2.5 PVs). Lastly, barium retention appeared to be constant throughout all flooding sequences after achieving steady state at 2.5 PVs.

Table 4.8: Average ion concentration after each flooding sequence in ME8

Flow rate [PV/day]	Average Ca^{2+} [mol/L]	Average Sr^{2+} [mol/L]	Average Ba^{2+} [mol/L]	Pore volumes injected interval [PVs]
1	0.0256	-0.0217	-0.0029	0.0 – 37.7
4	0.0256	-0.0219	-0.0034	37.8 – 73.1
1	0.0303	-0.0263	-0.0028	74.7 – 90.3
0.5	0.0320	-0.0275	-0.0025	90.9 – 94.6

After the data analysis was conducted, the calculated average calcium production was 0.0008 mol/L higher than retained strontium and barium, similar to ME22 calculations. However, reanalyzing effluent samples with a different standard could be interesting to try to reconstruct similar concentrations, especially barium concentrations. This is further discussed in section 5.4.

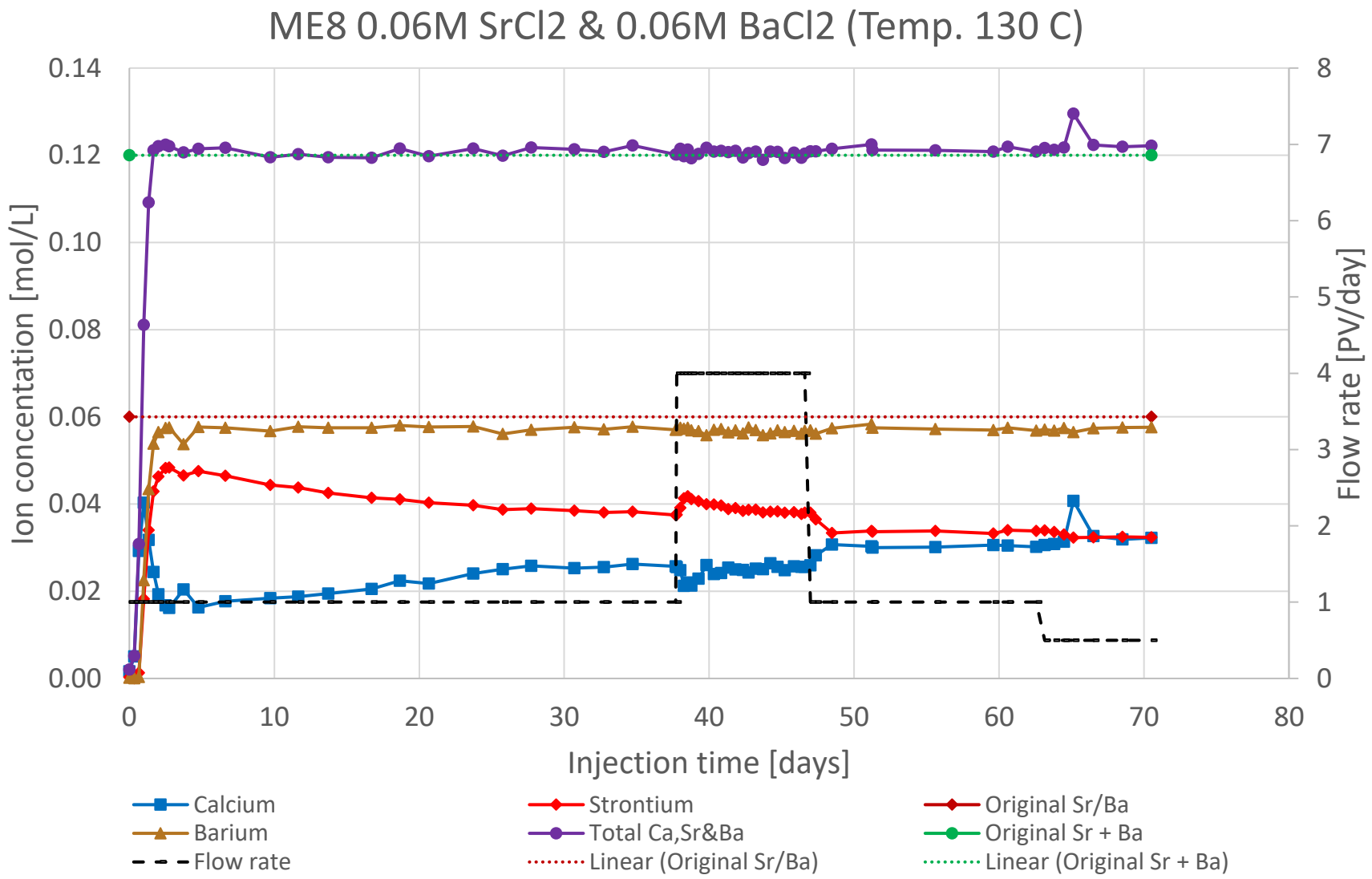

Figure 4.7: Analyzed effluent concentrations plotted against injection time in days

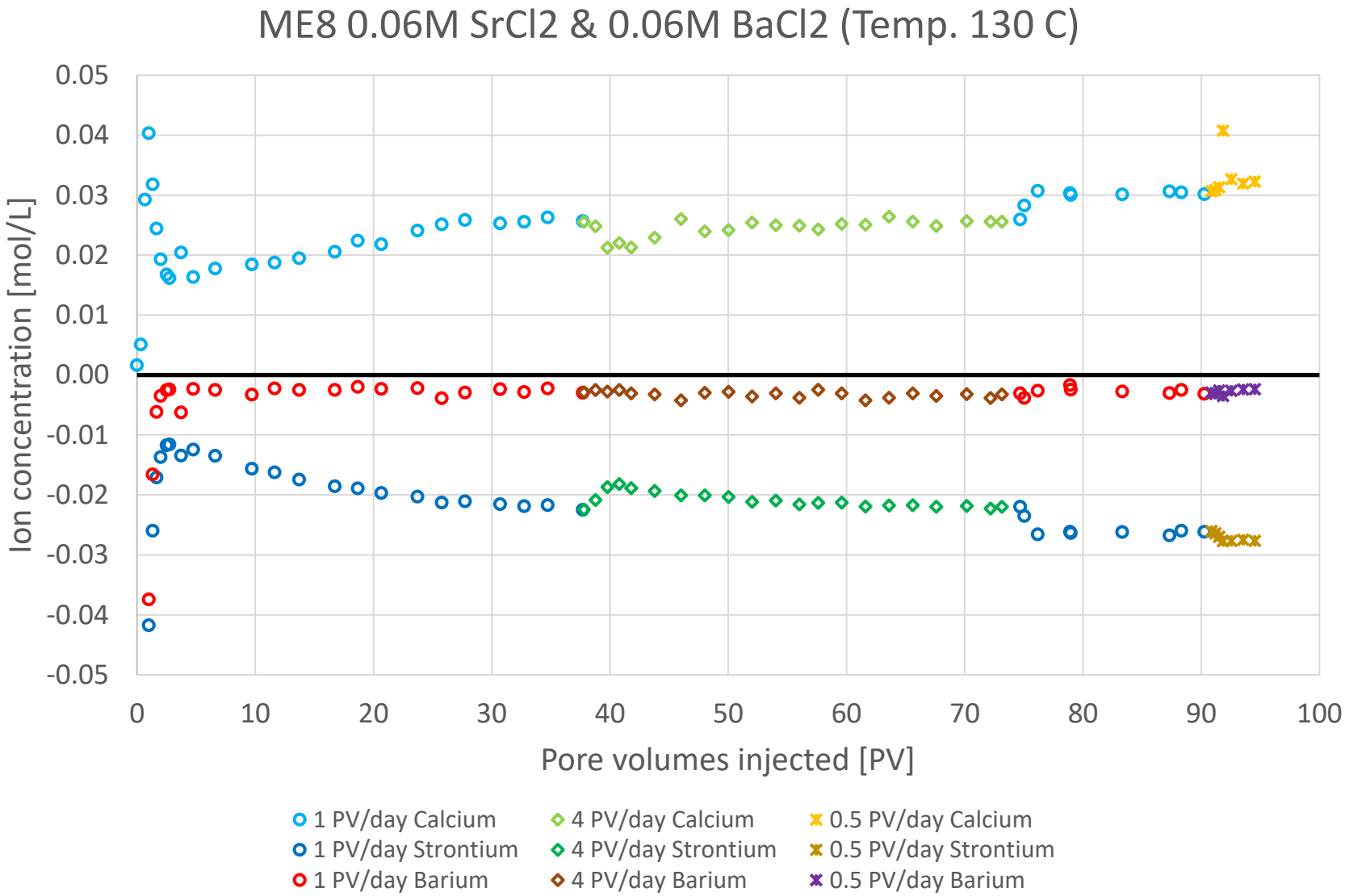

Figure 4.8: Measured strontium and barium minus the injected concentrations and calcium plotted against pore volumes injected

5. Discussion

All experiments proved a symmetric trend of the produced calcium from the chalk core and retained divalent ions from the injection brine. Loss of strontium and barium lead to an equal produced concentration of calcium which can be assumed as a substitution-like process, similar to previous experiments with magnesium (Korsnes et al., 2006; Madland et al., 2011; Andersen et al., 2022). A higher total calcium concentration was obtained compared to the lost brine ions. However, the differential was insignificant and assumed to be from chalk dissolution by the brine pH. Moreover, flooding with the combined divalent brine ions, i.e. strontium-magnesium, and strontium-barium showed to affect the steady state.

Upon discussing the results obtained from experiments in section 4, results from Korsnes and Madland (2017) and Andersen et al.'s (2022) experiments will also be presented to compare similarities and differences in their and our findings. Korsnes and Madland (2017) conducted their experiment with Mons chalk but had a higher confining pressure than used for our experiments. Andersen et al. (2022) investigated the rate dependency with Stevns Klint chalk and Kansas chalk with similar test conditions.

5.1. Strontium concentrations and reaction kinetics

The three experiments containing strontium in the brines (ME22, ME10 and ME8) measured a strontium retention between 36 and 59 % of the initial injection concentration. The lowest measured strontium retention was during the first 1 PV/day flooding with ME8, figure 4.8, and the highest measured was in ME10 during 0.5 PV/day flooding, figure 4.6.

5.1.1. Pure strontium-based brine

Only one experiment (ME22) was conducted with pure strontium-based brine. After the first flooding with 1 PV/day, the retained strontium percentage was measured at 57 % of the brine's initial concentration. All the other flooding sequences changed the retention by only ~5 %, table 4.1. However, all flooding rates showed that more than 50 % of the injected strontium

precipitated inside the chalk core. As reactive flooding was initiated, the strontium brine took approximately 20 PVs to reach a steady state and collected data beyond 20 PVs were used to calculate the average steady state concentration, figure 4.2. As flow rates increased, strontium retention and calcium production decreased. Similar observations were conducted on magnesium-based brine (Andersen et al., 2022). Increased flow rate gives the brine less time to react upon the core, leading to less retained strontium and produced calcium. As the flow rate was set to 1 PV/day a second time, after injecting higher flow rates, the retained strontium and calcium concentration return to similar concentrations observed during the first 1 PV/day flooding, figure 4.2. Reducing the flow rate to 0.5 PV/day increased calcium production. However, strontium remained unchanged, table 4.1. The initial data with 0.5 PV/day was measured to be scattered and, therefore, should be reanalyzed, figure 4.1. By the strontium retention observations with previous flow rates and the increase in calcium production at 0.5 PV/day flooding, indicates the retained strontium increased with similar rate as calcium. The last 1 PV/day is excluded from the discussion due to the short flooding duration.

The observation of pure strontium-based brine shows that reaction kinetics was affected with flow rate changes. Increasing the flow rate led to a decrease in strontium retention, and flooding 1 PV/day a second time measured comparable concentrations observed during the first phase of 1 PV/day. Interestingly, Andersen et al. (2022) observed higher retained magnesium and produced calcium during the second phase of 1 PV/day with Kansas chalk. Similar results were observed in Stevns Klint chalk (SKA1). Thus, strontium appears more stable due to returning to previous flooded flow rates determined to duplicate similar concentrations. Another observation when comparing magnesium-based and strontium-based brines are the retained brine ions. Throughout the first ~120 days for Kansas and Stevns Klint chalk with magnesium, 8 – 14 % of the original brine concentration was retained. It should be acknowledged that higher magnesium retention was observed beyond 120 days of flooding, but no comparable results with observation measured from ME22 (more than 50 %). Korsnes and Madland (2017) retained approximately 2/3 of the original strontium concentration with 1 PV/day flooding. However, as mentioned, over 400 days with magnesium brine were flooded before strontium was injected, and the confining pressure was higher during their experiment. Upon injecting strontium brine in their study, a similar-sized production of magnesium and calcium ions was measured in the effluent samples. Thus, precipitated magnesium inside the core or/and increased confining

pressure appears to affect the reaction kinetics of rock-fluid interaction, increasing the retained strontium with flooding.

5.1.2. Strontium in strontium-barium/magnesium brine

Initial flooding for ME10, 1 PV/day with strontium-magnesium brine, showed lower strontium loss. 45 % of strontium's initial concentration was retained. Subsequently, after first flooding with 1 PV/day for ME8, strontium retained lower than ME22 and ME10 with a 36 % retention of initial concentration. Achieving steady state for ME10 seems to occur at similar pore volumes injected as ME22. After 20 PVs, effluent magnesium concentration reached its original concentration and stayed constant for the remainder of the experimental testing, figure 4.6. Strontium concentrations stabilized when magnesium concentration returned to its initial brine concentration. ME8 required a longer flooding duration to acquire a steady state. Upon breakthrough of original sodium and chloride concentrations, barium stabilized at a ~5 % retention with insignificant changes through the first phase of 1 PV/day flooding, figure 4.8. As flooding continues, strontium and calcium do not reach a steady state until 27 PVs are injected. It appeared that the barium in the injection brine influenced the time to acquire steady state for strontium.

Increasing the flow rate led to similar strontium retention and calcium production trends for ME10 and ME8. Upon increasing the flow rate to 4 PV/day, a drop in calcium production and strontium retention were measured. Meanwhile, magnesium and barium concentrations remain adequately unchanged. As further flooding proceeded, an increasing trend for calcium production and strontium retention was measured, figure 4.6 and figure 4.8. The increasing trend with increasing flow rate deviated from data obtained from ME22 and Andersen et al. (2022). As flow rates increase, strontium retention and calcium production should decrease. With an increased flow rate, the residence time of brine to interact with the chalk core decreases and should lead to a decrease in produced calcium and retained strontium. It is uncertain what was causing this increasing trend in the dissolution of calcium and increased precipitation of strontium-bearing minerals during 4 PV/day flooding.

The second phase of 1 PV/day flooding increased calcium production and strontium retention after flooding with 4 PV/day for ME10 and ME8. Furthermore, ME10 and ME8 obtained higher calcium production and strontium retention compared to the first phase of 1 PV/day, figures 4.6

and 4.8. Similar observations were conducted in magnesium, Andersen et al. (2022). Upon injecting 1 PV/day a second time, higher retention of magnesium was observed for Stevns Klint and Kansas chalk. An interesting result was measured in ME10 during the second phase of 1 PV/day. After flooding with 1 PV/day a second time, the retention of strontium was similar to the results from ME22, approximately 57 %. Thus, after flooding 85-90 PVs in ME10, similar retained strontium values were achieved in ME10 and ME22. ME8 strontium retention increased from 36 % to 45 % during its second injection phase at 1 PV/day. However, ME8 was the only experiment with two active ions precipitating inside the core: strontium and barium. Adding the retained concentration of barium and strontium from the initial brine concentration led to 50 %, 45 % from strontium, and 5 % from barium. Hence, the total precipitation concentration in ME8 was still lower than ME22 and ME10. Lastly, decreasing the flow rate to 0.5 PV/day led to the highest calcium gain and strontium loss for ME10 and ME8. The measured strontium retention was 59 % and 46 % for ME10 and ME8, respectively.

Results measured from ME10 indicate no precipitation of magnesium occurred when flooding with equal concentrations of strontium and magnesium in the brine. Initially, precipitation of magnesium was observed in the first 20 PVs before effluent magnesium concentrations stabilized towards original brine concentration in the remainder of the flooding, figure 4.6. After that, the reaction kinetics between brine and rock are dominantly from strontium in the injection brine and calcium from the chalk core. The dominating reaction kinetics between calcium and strontium over magnesium observed from ME10 and the back-produced magnesium ions upon injecting strontium brine in Korsnes and Madland' (2017) study; could suggest that precipitated magnesium-bearing minerals inside the chalk will be substituted with strontium-bearing minerals. Not only calcium.

5.1.3. Strontium comparison

It is discussed if reaction kinetics in strontium is more affected by the presence of other divalent ions in the brine or bearing minerals in chalk than the flow rate at 130 °C. The experiments conducted in this thesis observed a ~5 % difference in strontium retention with pure strontium-based brine at different flow rates (between 0.5 and 8 PV/day), figure 4.2. Flooding with strontium-magnesium (ME10) appeared to increase the injection time required to obtain similar strontium retention, while flooding strontium-barium seemed to decrease the overall strontium

retention. After the first flooding sequence, 1 PV/day, ME10 measured 12 % less strontium retention than ME22, figures 4.2 and 4.6. After injecting 85-90 PVs and flooding 1 PV/day a second time could similar strontium retention results be obtained in ME10 as in ME22. Flooding with strontium-barium brine required a longer flooding duration for strontium to reach a steady state compared to ME22 and ME10. The strontium retained after the first and second flooding of 1 PV/day was measured 21 % and 12 % lower than ME22, respectively, figure 4.8. Nevertheless, none of the experiments managed to retain similar strontium retention as observed in Korsnes and Madland (2017). Therefore, could the precipitated magnesium-bearing mineral inside the core in Kornes and Madland (2017) have a positive effect on strontium retention, thereby being the reason higher strontium retention was observed in their study with 1 PV/day flooding? Or was the highest strontium retention never obtained during our experiments?

5.2. Barium concentrations and reaction kinetics

A remark upon flooding with barium-based brines (ME18 and ME8) was the quick steady state determination. When regaining initial concentrations of sodium and chloride, barium showed insignificant changes during the first phase of 1 PV/day flooding for both ME18 and ME8. Additionally, the retained barium was lower than strontium retention and more comparable with magnesium retention in Andersen et al. (2022). Lowest and highest retained barium was 0.5 PV/day flooding in ME8 and 0.5 PV/day flooding in ME18 measuring 4 % and 16 % of initial brine concertation, respectively, figures 4.8 and 4.4. Andersen et al. (2022) measured magnesium retention between 8 – 14 % of the original concentration at different flow rates for the first 120 days. Their experiments continued beyond 120 days, where the retained magnesium increased. However, it will not be used in this comparison, as the longest experiment conducted for this thesis was conducted for 110 days. Korsnes and Madland (2017) injected 0.06 mol/L barium-based brine after strontium-based brine had been injected and a second time after calcium-based brine had been injected.

5.2.1. Pure barium-based brine

ME18 was the only core that was flooded with pure barium brine. After the first phase of 1 PV/day, 10 % of barium was retained at a steady state. After achieving steady state flow rate

was increased. All increased flow rates, meaning 2, 4, and 8 PV/day, initially started with a drop in retained barium, followed by an increasing barium retention trend. 2 PV/day stabilized towards steady state concentration retained in previous flooding, 1 PV/day, table 4.4. However, 4 PV/day and 8 PV/day flooding, measured a barium retention increase of 0.0013 mol/L per 10 PVs injected after the initial drop in barium retention, and showed no indication of stabilizing before the flow rate was changed, figure 4.4. Thus, a failure to achieve steady state for both flooding sequences. It is suggested that the increase would continue until similar concentrations contained during the second phase of 1 PV/day flooding were reached.

Upon reduction in flow rate to 1 PV/day, a second time, an increase was detected for produced calcium and retained barium, thereafter, providing insignificant changes in concentrations. This led to barium retention of 16 % of its initial concentration. As earlier mentioned in section 5.1.2. a higher magnesium retention was observed during second phase of 1 PV/day flooding in Andersen et al. (2022). The difference between magnesium and barium observations was by flow rates greater than 1 PV/day. Increasing the flow rate with magnesium-based brine led to a decrease in retained magnesium and calcium. Barium measured an increasing retention trend with increased flow rate and measured calcium production with a similar rate. Hence, barium appears to deviate from the data obtained from ME22 and Andersen et al. (2022). Log data were analyzed to investigate what caused the increase in retention of barium with increased flow rate. Nevertheless, no clear explanation could determine what was causing the increase in retention. It was proposed that the increasing flow rate, and also increases differential pressure, displaces the brine into unflooded zones. Therefore, increasing the chalk surface upon barium can react, but this could not be proven. Furthermore, the second phase with 1 PV/day in ME18 showed comparable measurements with Korsnes and Madland's (2017) second barium flooding. During their second barium injection, after injecting calcium brine, retained barium was measured to be approximately 0.01 mol/L. This was calculated to be approximately 16 % of the initial brine concentration. Furthermore, the back-produced ions were dominated by calcium. The retained barium in their first flooding was approximately 1/3 of the original brine concentration. However, magnesium and small concentrations of strontium were back-produced along with calcium ions, which may have affected the retained barium concentrations. Reducing the flow rate to 0.5 PV/day in ME18 proved comparable with the theory. Increasing the residence time increased the retained barium and produced calcium.

5.2.2. Barium in strontium-barium brine

Barium in flooding with strontium-barium brine (ME8) determined to be relatively constant throughout the entire flooding. After obtaining initial concentrations of sodium and chloride, barium retention was ~5 % of the initial brine concentration, and the other flooding sequences changed the retention by only ~1 %, figure 4.8. It is discussed whether the meager change in barium retention with each flooding sequence is an outcome of uncertainties—the difference in the highest and lowest barium retention averages less than 0.001 mol/L, table 4.8. If the measured data was realistic, barium retention was at its highest during 4 PV/day flooding and lowest during 0.5 PV/day flooding. At the initial flooding phase with 4 PV/day, a drop in retained strontium was measured, between 40 – 55 PVs injected, before gradually stabilizing towards steady state comparable with the previous flooding, 1 PV/day, figure 4.8. Furthermore, the lowest barium retention was measured during 0.5 PV/day flooding, and retained strontium was at its highest (92-95 PVs). It appears barium retention correlates with strontium retention. Upon retaining less strontium, higher barium retention was measured, and as strontium retention increases, barium retention decreases.

5.2.3. Barium comparison

ME18 suggests pure barium-based brine is affected by flow rate but uncertain to what extent. In retrospect, further flooding investigation should have been conducted on ME18 before ending the experiment. The data from ME18 suggest an increasing trend in barium retention with higher than 1 PV/day flooding, data from 30 to 110 PVs, figure 4.4. As this deviate from theory and previous observation from strontium and magnesium flooding, it is uncertain whether an increased flow rate will increase barium retention. Moreover, similar barium retention from Korsnes and Madland (2017) was achieved, 16 % retained from the brine's initial concentration. The writer asks if an increase in flow rate after retaining 16 % of the original barium concentration leads to similar flow rate trends as in ME22, a drop in barium retention and reaching a plateau. Alternatively, would the retained barium continue to increase? The data third phase with 1 PV/day perceives to decrease in barium retention and calcium production. However, due to the short flooding duration of three days it is uncertain to conclude how the barium retention would evolve with continues flooding.

It is recommended to investigate different flow rates for ME8. Due to the small comparison of 0.5 and 4 PV/day it is uncertain about concluding if the barium retention was affected by the flow rate. Could there be a dependency in barium retention with higher or lower flow rates. Or is there a correlation between strontium retention and barium retention, i.e. does lower strontium retention lead to higher barium retention. Moreover, a similar observation was conducted in ME10. Small magnesium retention was observed after increasing the flow rate to 4 PV/day and a drop in strontium retention was measured (between 40 and 45 PVs in figure 4.6.). In other words, as strontium retention decreases, will barium retention increase?

5.3. Core findings

The data collected from strontium and barium brine proved to correlate accurately with the core mass increase. The difference in calculated from IC analysis and actual mass increase was 0.03 g and 0.30 g for ME22 and ME18, respectively. Subsequently showed clear indication that highest retention with brine and chalk occurred in the presence of strontium (ME22). Strontium has an atomic mass of 87.62 g/mol, and barium has an atomic mass of 137.33 g/mol. Even though strontium has a lower atomic mass than barium, a higher mass increase was measured on ME22, 10.6 grams more than ME18. The densities were also calculated to be higher at the inlet for ME22. ME22 obtained an estimated inlet density of 3.60 g/cm^3, appendix A. Density of pure strontium carbonate ($SrCO_3$) is 3.71-3.74 g/cm^3. Implies the inlet piece R_1 in ME22 was almost pure $SrCO_3$. SEM analysis confirmed this, where 11 spot analyses were conducted on the R_1 piece. The analysis confirmed that the inlet slice had only a small weight percentage of Ca, ranging between 1.47 to 3.55 %. The rest of the weight percentage persisted of Sr, C, and O ions. An interesting observation when conducting the SEM analysis was that areas that were expected to contain calcium proved to be strontium. SEM analyses were also conducted on the outlet slice of the ME22 core, and the analysis proved no indication of strontium precipitation.

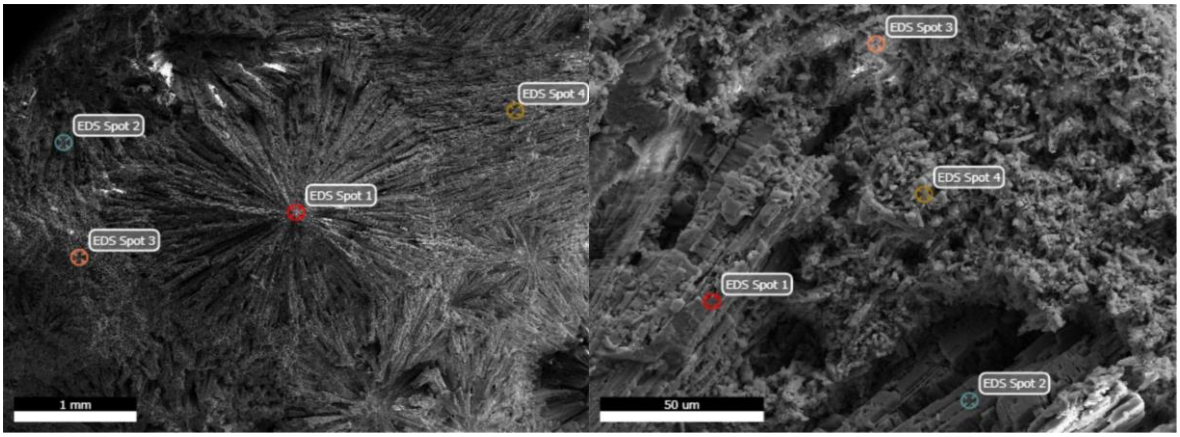

Figure 5.1: SEM pictures of precipitated strontium carbonates at the inlet slice R_1, ME22

SEM of ME18 was also conducted, where a piece of the inlet (R_1) and outlet were analyzed, appendix B. As barium carbonate has a density of ~4.29 g/cm^3 and a calculated density of the inlet pieces R_1 was 3.19 g/cm^3, it was expected to find a mixture of barium carbonate and calcium carbonate. Upon inspecting the inlet of ME18, a clear separation of barium precipitation and calcium carbonate was discovered through the microscope. Indicating precipitation of barium occurred only at the inlet and appeared to move as a front inward the core. Observing the core and the SEM analysis, the precipitation front appeared at the transaction from decolorization, a gray area, of the inlet. The analysis of the core's white chalk indicated insignificant barium carbonate results. Lastly, analyzing the outlet of ME18 showed no precipitation of barium.

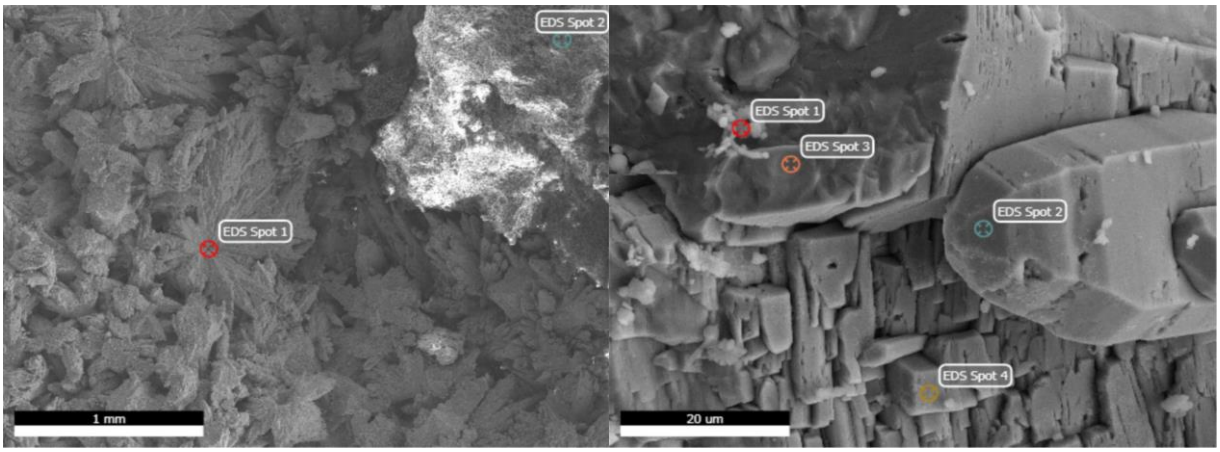

Figure 5.2: SEM pictures of precipitated barium carbonates at the inlet slice R_1, ME18

ME22 and ME18 SEM and density calculations of the core pieces for both cores confirm that precipitation occurred at the inlet. For ME22, due to the high percentage of retained strontium ions, the precipitation of strontium carbonate had moved further into the core compared to ME18. Furthermore, the SEM did not analyze the discolored front of ME22, being R_2 or L_1, appendix A.

Korsnes and Madland's (2017) observations on precipitation of strontium and barium carbonates can make the chalk mechanically stronger. However, as the precipitation occurs at the inlet of the chalk core and no precipitation at the outlet suggests the formation becomes mechanically stronger where the precipitation occurs, at the inlet. Moreover, the chalk flooded zones with no proven strontium or barium carbonates precipitation should retain similar properties to initial chalk.

5.4. Uncertainties affecting the results

Brine analysis will always create uncertainties in the data collection, either human error, machine failure/inefficient use in machinery, or poorly cleaned equipment. The highest uncertainties remain during the procedures conducted before the IC analysis, as the IC analysis can duplicate comparable results from the same sample. Uncertainties in data analysis provided in this experimental test can be an occurrence of:

- Poorly cleaned equipment
- Incorrect dilution ratio from liquid handling machine or IC machine
- Inaccurate standards used for calculating effluent concentrations

IC analysis emphasizes the analyzed data, so the error margin needs to be discussed. Three vials are used before IC analysis is conducted, a sampling vial, a vial for 1000x diluted effluent sample, and a plastic vial fit for the IC machine. However, even if the vial is cleaned, small containments of salt may be present, e.g., cracks in the vial glass or vial is not properly washed. Either way, if one of the vials is proven unclean, it will affect concentration calculations from IC analysis. Furthermore, with a concentration of 0.12 mol/L diluted 1000x, the smallest containment of salts will affect the analysis.

In the process of diluting effluent samples, air bubbles in the tubing can create inaccurate mixing ratios, which will increase the intended salt concentration of its sample. Air bubbles can also occur in the IC machine when injecting a sample into the columns. Thus, the liquid handling- and IC machine were primed before use to prevent the air inside the tubes and syringes. However, inaccuracies in the mixing ratios from the liquid handling machine or the IC machine are detectable, thus, simple to eliminate from further calculations. The data point, from figure 4.1, at approximately 34 days, may result from inaccuracies in the mixing ratios, as all ions (including sodium and chloride) were significantly higher than other data samples. Unclean vial and air in the tubing will affect one of the many samples analyzed, and reanalyzing the sample will correct the data error. However, reanalyzing samples is time-consuming, and not all data could be corrected due to time limitations. An exception is, that if the sampling vial is unclean, reanalyzed samples will not correct the data error.

Before concentration calculations, equation 2.9a was used for all standards to evaluate the linear relationship and credibility between ion concentration and its area provided by the IC analysis. In addition, due to the standards' importance, two vials were prepared and analyzed for each standard in case of receiving incorrect values (e.g., unclean vial). SSW standard and originally injected brine were fixed. Lastly, the third standard, $CaCl_2$ mixed with divalent ions from the injected brine, was mixed to desired concentrations. Due to the linearity relationship between measured area and concentration, this standard should be mixed as close to the concentrations of the effluent samples to create accurate concentrations. The $CaCl_2$ standard used for ME10 (0.06 mol/L $MgCl_2$ & $SrCl_2$) and ME8 (0.06 mol/L $SrCl_2$ & $BaCl_2$) were mixed to 0.04 mol/L with Ca, Sr and Mg/Ba. The measured effluent concentration in ME10 was 0.06 mol/L, ~0.025 mol/L, and ~0.035 mol/L with Mg-, Sr-, and Ca-ions, respectively, figure 4.5. The measured effluent concentration in ME8 was 0.055 mol/L, ~0.035 mol/L, and ~0.03 mol/L with Ba-, Sr-, and Ca-ions, respectively, figure 4.7. Hence, a more appropriate standard for ME10 and ME8 would be a mixture of 0.06 mol/L with Mg/Ba, and 0.03 mol/L with Sr and Ca. Therefore, it is suggested in future work with similar injection brines that the effluent calculations are conducted with the suggested standards above and observe if the concentrations will lead to better CBE values.

IC analysis can create uncertain or incorrect results. Hence, some reruns of effluent samples were conducted. Uncertain data were conducted to try and replicate the same results as previous. Incorrect results, occurrence by human or machine error corrupting the analysis, were reanalyzed to correct the error. If the uncertain or incorrect results could not be corrected due to this experiment's time limitation, these data were excluded from further average calculations provided in this thesis. Hence, LMA and CBE were conducted for every effluent sample analyzed to judge the validity and quality of the data results. Higher deviation of LMA and CBE resolved in effluent data being excluded in further calculations.

When ME22 and ME18 were finished, new saturated and dry mass measurements were conducted. In order to perform these measurements, the distribution plate, rubber gasket, and shrinking sleeve had to be removed. In the removal of these experimental parts, small chunks of chalk were still attached to them. Hence, the saturated mass of the core, distribution plates, rubber gasket, and the shrinking sleeve were measured separately. Similar measurements were conducted for dry masses. After attaining dry mass measurements, the equipment was washed to remove all chalk from them, and then all parts were dried and measured again. The difference in mass, with and without chalk, was added to the dry mass to obtain a total dry mass. However, this could not be applied when measuring the saturated mass of the core. Thus, a correlation between the saturated and dry mass of the core was calculated. Then the correlation was applied to the mass of chalk attached to the equipment to obtain a total saturated mass of the core. Using a correlation instead of exact measurements creates uncertainties. However, the error margin was predicted to be meager. Hence, the PoroPerm porosimeter was also used for more accurate measurements regarding density, porosity, and pore volume.

6. Conclusion

- The IC analysis showed a relative equal concentrations of produced calcium ions and retained brine ions. Furthermore, the effluent analysis of retained brine ions and produced calcium ions correlated with the measured core mass increase after flooding.
- Injecting strontium brine led to a retention of more than 50 % of the original concentration and changing the flow rate showed a ~5% difference strontium retention between 0.5 and 8 PV/day. Flooding with strontium-magnesium brine obtained strontium retention between 45-59 % and measured highest retention of original brine concentration. Additionally, strontium-barium brine measured the lowest strontium retentions, between 36-45 %.
- Injection barium brine measured comparable results with magnesium retention from previous study and measured barium retention between 8-16 % of original brine concentration. In addition, at the second flooding with 1 PV/day, barium retention was comparable with previous barium injection study. Whereas strontium-barium brine measured relatively constant barium retention for all flooding sequences, approximately 5 %.
- Flooding only strontium brine appeared to response with the expected reaction kinetics by increasing the flow rate; decrease strontium retention and calcium produced. Increasing the flow rate with Ba-, Sr-Mg-, and Sr-Ba brines led to an unexpected increase in the brine retention, which could not be compared with previous studies. Furthermore, decreasing the flow rate created an expected increase in brine ion retention at steady state for all experiments.
- During second 1 PV/day flooding for Ba-, Sr-Mg-, and Sr-Ba resulted in higher brine ion retention which also had been observed in previous studies.
- Matrix density and SEM spot analysis was conducted on two cores and showed precipitation of strontium and barium carbonate occurred at the inlet. The analyzed inlet slice in the strontium flooded core was almost completely converted to $SrCO_3$. Whereas a mixture of precipitated $BaCO_3$ and initial $CaCO_3$ was found at inlet in the barium flooded core, due to the low retention in barium flooding.

7. Future work

- Future work should continue to investigate how various flow rates affect the concentrations for ME10 and ME8 when strontium is flooded with either magnesium or barium. It would be suggested to investigate higher flow rates such as 8 PV/day, with both tests to observe how the data resolve. Will retention of strontium increase as observed in previous floodings with 4 PV/day, or will the data provide a decrease with a plateau as observed in ME22.
- Future studies should also continue investigate how the precipitation of strontium and barium carbonate are further into the chalk cores. How is the transition between an area where there are newly precipitated minerals and the areas where no visible precipitation have taken place. Is there an abrupt precipitation front? Are all discolored areas mainly strontium and barium carbonate as observed at the inlet or does the precipitation partly fade into the core?

A. ME22 core after flooding with 0.12 mol/L $SrCl_2$

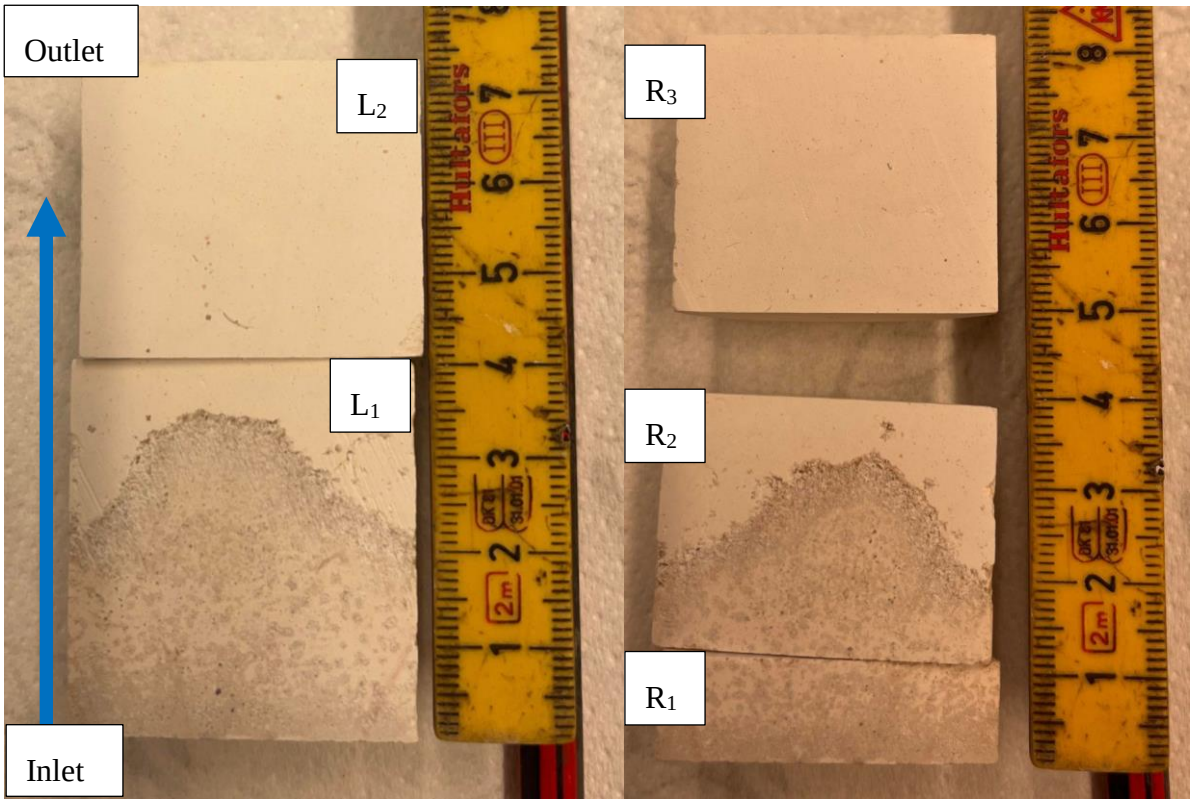

Figure A.1: Core cuts of ME22 after flooding, subdivided into L_1, L_2, R_1, R_2, & R_3

B. ME18 core after flooding with 0.12 mol/L $BaCl_2$

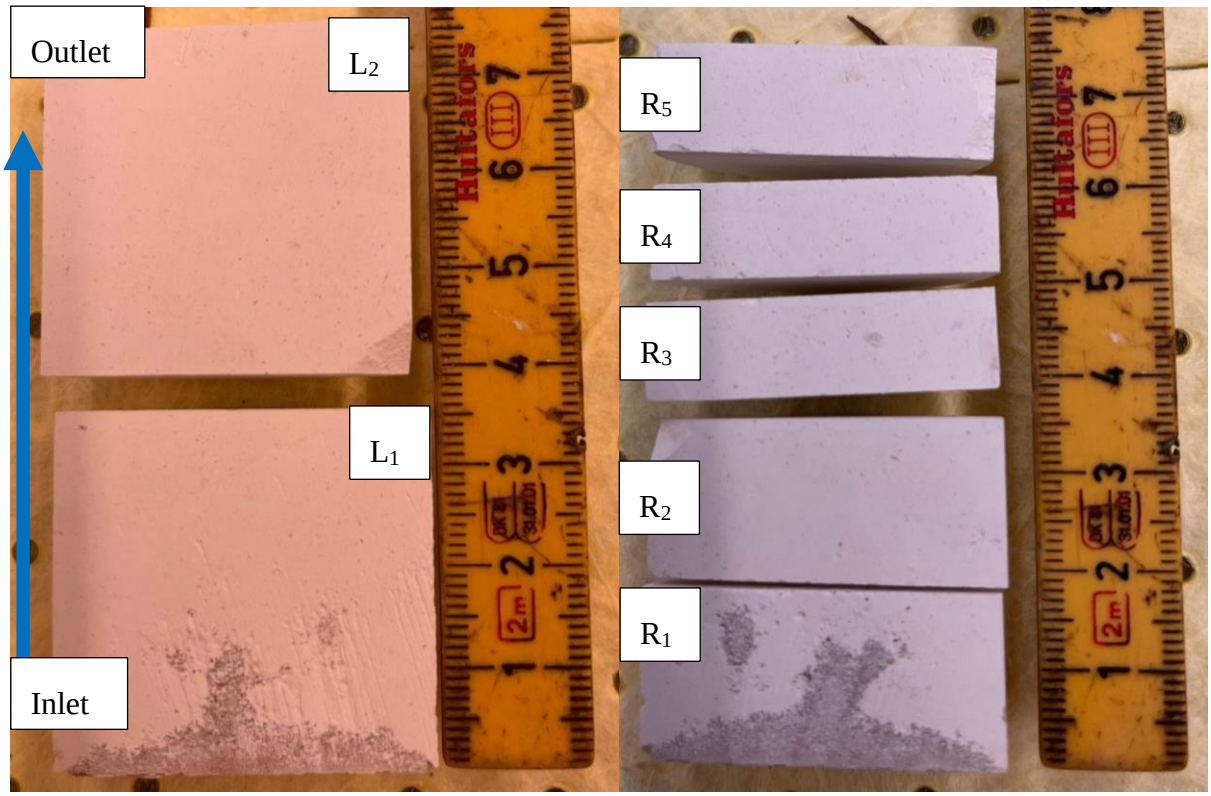

Figure B.1: Core cuts of ME18 after flooding, subdivided into L_1, L_2, R_1, R_2, R_3, R_4 & R_5

References

Andersen, P. Ø., & Berawala, D. S. (2019). Modeling of creep-compacting outcrop chalks injected with Ca-Mg-Na-Cl brines at reservoir conditions. *SPE Journal, 24 (6)*, 2889-2910.

Andersen, P. Ø., Korsnes, R. I., Olsen, A. T., & Bukkholm, E. T. (2022). Reaction kinetics determined from core flooding and steady state principles for Stevns Klint and Kansas chalk injected with MgCl2 brine at reservoir temperature. *SPE Journal*, 1-20. doi:https://doi.org/10.2118/209380-PA

Appelo, C. A., & Postma, D. (2005). *Geochemistry, groundwater and pollution (2nd ed.).* Great Britain: A.A. Balkema Publishers.

Barium chloride dihydrate; MSDS No. 101719. (Accessed 2022, June 6). Merck KGaA: Darmstadt, Germany, December 1, 2021. Retrieved from https://www.merckmillipore.com/NO/en

Bjorlykke, K. (2015). *Petroleum Geoscience: From sedimentary enviromentss to rock physics (2nd ed.).* Berlin: Springer-Verlag.

Brezonik, P. L., & Arnold, W. L. (2011). *Water chemistry: An introduction to the chemistry of natural and engineering aquatic systems.* United States: Oxford University Press.

Brown, T. L., LeMay, H. E., Bursten, B. E., Murphy, C. J., & Woodward, P. M. (2012). *Chemistry: The central science (12th ed.).* United States: Pearson Prentice Hall.

Bukkholm, E. T. (2021). *Reactive flow in chalk at reservoir temperature – Experiment and simulation.* [BSc thesis, University of Stavanger]. Retrieved from https://hdl.handle.net/11250/2774453

Dalefield, M., Nguyen, L., Zheng, Z., & Naiman, C. (2022, April 11). *OSU Chemistry REEL Program*. Retrieved from OSU Chemistry Education:

https://research.cbc.osu.edu/reel/research-modules/environmental-chemistry/instrumentation/instrument-calibration/ion-chromatography-theory/

Doornhof, D., Kristiansen, T. G., Nagel, N. B., & Sayers, C. (2006). Compaction and subsidence - Schlumberger. *Oilfield Review, 18*, 50-68.

Hermansen, H., Landa, G. H., Sylte, J. E., & Thomas, L. K. (2000). Experiences after 10 years of waterflooding the Ekofisk field, Norway. *Journal of Petroleum Science and Engineering, 26 (1-4)*, 11-18. doi:https://doi.org/10.1016/S0920-4105(00)00016-4

Kamel, N., & Ashry, A. (2011). Ground water in certain sites in Egypt and its treatments using a new modified ion exchange resin. *Journal of Enviromental Protection, 2*, 435-444. doi:10.4236/jep.2011.24050

Korsnes, R. I., & Madland, M. V. (2017). The effect on compaction rates by divalent anion and cations on outcrop chalk tested at reservoir temperature and effective stress conditions. *American Society of Civil Engineering*, 706-714.

Korsnes, R. I., Strand, S., Hoff, Ø., Pedersen, T., Madland, M. V., & Austad, T. (2006). Does the chemical interaction between seawater and chalk affect the mechanical properties of chalk. *Proceedings of the International Symposium of the International Society for Rock Mechanics* (pp. 427-434). Belgium: Eurock.

Madland, M. V., Hiorth, A., Omdal, E., Megawati, M., Hildebrand-Habel, T., Korsnes, R. I., . . . Cathles, L. M. (2011). Chemical alterations induced by rock-fluid interactions when injection brines in high porosity chalks. *Transport in porous mediia, 87*, 679-702.

Megawati, M., Hiorth, A., & Madland, M. V. (2013). The impact of surface charge on the mechanical behavior of high-porosity chalk. *Rock Mechanics and Rock Engineering, 46*, 1073-1090.

Megawati, M., Madland, M. V., & Hoirth. (2015). Mechanical and physical behavior of high-porosity chalks exposed to chemical perturbation. *Journal of Petroleum Science and Engineering, 133*, 313-327. Retrieved from 10.1016/j.petrol.2015.06.026

Minde, M. W. (2018). *Mineral replacements in flooding experiments linked to enhanced oil recovery in chalk.* [Doctoral dissertation, University of Stavanger]. Retrieved from https://uis.brage.unit.no/uis-xmlui/handle/11250/2578165

Mokhtari, R., Anabaraonye, B. U., Afrough, A., Mohammadkhani, S., & Feilberg, K. L. (2022). Experimental investigation of low salinity water-flooding in tight chalk oil reservoirs. *Journal of Petroleum Science and Engineering, 208*, Article 109282. doi:https://doi.org/10.1016/j.petrol.2021.109282

Nagel, N. B. (2001). Compaction and subsidence issues within the petroleum industry: From Wilmington to Ekofisk and beyond. *Physics and Chemistry of the Earth, Part A: Solid Earth and Geodesy, 26 (1-2)*, 3-14. doi:https://doi.org/10.1016/S1464-1895(01)00015-1

Nermoen, A., Korsnes, R. I., Hiorth, A., & Madland, M. V. (2015). Porosity and permeability development in compacting chalks during flooding of nonequilibrium brines: Insights from long-term experiment. *Journal of Geophysical Research: Sloid Earth, 120*, 2935-2960. doi:10.1002/2014JB011631

Oljedirektoratet. (2022, June 6). *Norsk Petroleum*. Retrieved from https://www.norskpetroleum.no/fakta/felt/ekofisk/

Olsen, A. T. (2020). *Reactive flow in chalk at reservoir condition.* [Unpublished BSc thesis]: University of Stavanger.

Rendel, P. M., Mountain, B., & Feilberg, K. L. (2022). Fluid-rock interaction during low salinity water flooding of North Sea chalk. *Journal of Petroleum Science Engineering, 214*, Article 110484. doi:https://doi.org/10.1016/j.petrol.2022.110484

Sachdeva, J. S., Nermoen, A., & Korsnes, R. I. (2019). Impact of initial wettability and injection brine chemistry. *Transport in Porous Media, 128*, 755-795.

Sachdeva, J. S., Nermoen, A., & Korsnes, R. I. (2020). Effect of initial wettability on rock mechanics and oil. *Transport in Porous Media, 133*, 85-117.

Sulak, R. M. (1991). Ekofisk field: The first 20 years. *Journal of Petroleum Technology, 43 (10)*, 1265-1271.

Sulak, R. M., & Danielsen, J. (1989). Reservoir aspects of Ekofisk subsidence. *Journal of petroleum techonolgy, 41 (7),* 709-716.

Swapp, S. (2022, May 26). *Geochemical Instrumentation and Analysis*. Retrieved from The Science Education Resource Center: https://serc.carleton.edu/research_education/geochemsheets/techniques/SEM.html

Sylte, J. E., Thomas, L. K., Rhett, D. W., Bruning, D. D., & Nagal, N. B. (1999). Water induced compaction in the Ekofisk field. *SPE Annual Technical Conference and Exhibition.* Houston, United States: Society of Petroleum Engineering.